Hindawi
Structural Control and Health Monitoring
Volume 2023, Article ID 3754773, 19 pages
https://doi.org/10.1155/2023/3754773

Research Article

A Novel Integrated Optimization-Driven Design Framework for Minimum-Weight Lateral-Load Resisting Systems in Wind-Sensitive Buildings Equipped with Dynamic Vibration Absorbers

Zixiao Wang and Agathoklis Giaralis

Department of Engineering City, University of London, London, UK

Correspondence should be addressed to Agathoklis Giaralis; agathoklis@city.ac.uk

Received 14 September 2022; Revised 9 November 2022; Accepted 24 November 2022; Published 24 February 2023

Academic Editor: Yi-Qing Ni

The increasing rate of urbanization in recent decades has resulted in a global surge in the construction of slender high-rise buildings. These structures are prone to excessive wind-induced lateral vibrations in the crosswind direction owing to vortex shedding effects, causing occupant discomfort and, ultimately, dynamic serviceability failure. To reconcile the worldwide accelerated trend in constructing tall buildings with the sustainable building sector agenda, this paper proposes a novel bi-objective integrated design framework that leverages dynamic vibration absorbers (DVAs) to minimize the required material usage in the wind load-resisting structural systems (WLSSs) of occupant comfort-governed tall buildings. The framework couples structural sizing optimization for minimum-weight WLSS design (objective 1), with optimal DVA tuning for floor acceleration minimization to satisfy codified wind comfort design requirements by using the smallest DVA inertia (objective 2). Furthermore, a versatile numerical strategy is devised for the efficient solution of the proposed bi-objective optimization problem. For illustration, the framework is applied to a 15-storey steel building equipped with one of two different DVAs: a widely considered top-floor tuned mass damper (TMD) and an innovative ground-floor tuned inerter damper (TID). The derived Pareto optimal integrated (WLSS-plus-DVA) designs demonstrate that significant reduction in both structural steel usage and embodied carbon emissions can be achieved using either one of the two DVAs with moderate inertia. It is concluded that the proposed optimization-driven design framework and numerical solution strategy offer an alternative innovative approach to achieve material-efficient high-rise buildings under wind hazards.

1. Introduction and Motivation

In recent decades, height-wise urban development has dominated the expansion in many major cities worldwide to accommodate pressing housing and office space demands posed by ongoing urbanization and population growth [1, 2]. Such development relies on slender high-rise buildings, which make efficient use of high-premium lands in congested urban environment. However, as their slenderness (height-to-width) ratios increase, high-rise buildings become particularly susceptible to aerodynamic forces in the crosswind direction due to the vortex shedding (VS) phenomenon, in which vortices are generated and shed periodically from one building side to the other creating alternating low-pressure zones [3]. These VS-induced forces may cause large sway oscillations in high-rise buildings even under frequently occurring moderate wind actions [4], leading to occupant discomfort and, ultimately, to downtime (serviceability failure) [5]. In this respect, meeting the occupant comfort serviceability criteria mandated by design building codes and guidelines (see, e.g., [6, 7]) becomes a critical design consideration for the lateral wind load-resisting structural system (WLSS) in VS-sensitive high-rise buildings [8, 9]. Examples of typical WLSSs for buildings of

up to about 25 storeys include moment-resisting frames, steel braced frames, and rigid frames coupled with reinforced concrete shear walls [10]. For taller buildings, commonly used WLSSs include steel outriggers and belt trusses, framed or trussed tubes, and diagrids. Usually, WLSSs are resisting gravitational loads as well, unless a separate gravity system is provided [10].

Meanwhile, the WLSS contributes significantly to the embodied carbon footprint (i.e., carbon emissions during material production, construction, maintenance, and demolition) of new-built high-rise buildings and, thus, to their overall environmental impact as the embodied carbon is becoming more important than operational carbon in modern energy-efficient buildings [11, 12]. In fact, the relative contribution of the WLSS to the overall embodied carbon of buildings increases rapidly with the building height as the design wind loads increase unfavourably with altitude [4], requiring heavier/stiffer WLSSs and thus higher material usage and heavier foundations. Specifically, Foraboschi et al. [13] reported an exponential relationship between building height and the overall environmental impact of high-rise buildings due to the increase in material requirements and structural member sizes of WLSSs with height. Furthermore, Gan et al. [14] demonstrated that the WLSS is the main contributor to the total embodied carbon in typical steel, reinforced concrete, and steel-concrete composite high-rise buildings, while Nadoushani and Akbarnezhad [15] found that decisions on WLSS design and material could result in 13.1–18.0% variation in the carbon footprint of mid-to-high-rise (i.e., 10-to-15 storey) steel and reinforced concrete buildings.

In this regard, given that about 11% of global greenhouse emissions are due to construction material production [16], the efficient material usage in the WLSS is critical not only for safeguarding occupant comfort and resilience of high-rise wind-sensitive buildings to wind loads but also for supporting environmentally sustainable height-wise urban development, with the aim of addressing the needs of the rapidly increasing global urban population, projected to almost double by 2050 [17]. In this setting, there is great scope for pursuing innovative and practically meritorious design protocols to minimize the required material usage in WLSS while satisfying the code-prescribed occupant wind comfort criteria in new high-rise wind-sensitive buildings.

To this end, dynamic vibration absorbers (DVAs), with the most representative embodiment being the passive tuned mass damper (TMD), are widely used to mitigate excessive VS-induced vibrations in tall/landmark buildings [18–20]. Specifically, the conventional TMD comprises a free-to-oscillate secondary mass attached to the building's top floor via stiffeners/springs and energy dissipation devices (e.g., viscous dampers) [21]. The stiffness and damping properties of the TMD are designed (tuned) to the fundamental lateral vibration mode of the building such that the inertia of the secondary mass is activated (i.e., the TMD oscillates), which counterbalances the wind-borne building oscillations and facilitates kinetic energy dissipation by the damping devices. By using an optimally designed TMD with a sufficiently large secondary mass, code-deficient tall buildings for occupant comfort can be retrofitted to meet the crosswind serviceability performance criteria [8]. Furthermore, recent research work demonstrated that inerter-equipped DVA, hereafter termed inerter-based vibration absorber (IVA), is a quite effective retrofitting solution to meet occupant comfort criteria in tall wind-sensitive buildings [22–25]. In typical IVAs [26–28], inertia is primarily endowed by inerter devices developing relative acceleration-resisting forces amplified through the inertance property [29], rather than by large oscillating mass blocks as in the TMDs. Relying on the fact that the inertance of experimentally verified inerter devices can readily scale up almost independently of the device physical mass using either mechanical gearing or fluid dynamics principles [30, 31], IVAs can achieve significant vibration suppression with much less additive weight and thus material use requirements, compared to TMDs.

Nevertheless, in routine high-rise buildings (e.g., 12–25 storeys), structural design engineers are used to meet code-specific, crosswind occupant comfort serviceability requirements by stiffening the WLSS instead of using TMDs, let alone IVAs. This approach is commonly supported by experiential trial-and-error WLSS design cycles [10]. Alternatively, automated WLSS sizing schemes involving the formulation and numerical solution of various constrained optimization problems for minimizing WLSS self-weight can be employed for the task [32–35]. However, increasing the stiffness of the WLSS to meet occupant comfort design requirements translates into higher construction material usage, especially since code-specific occupant comfort criteria generally become more stringent for stiffer structures [5]. In this context, WLSS stiffening in wind-sensitive high-rise buildings does not achieve material efficiency from the structural design viewpoint [36–38] which is recognized as a key step towards a net-zero economy [39, 40].

To this end, this paper proposes an innovative integrated design framework for VS-sensitive high-rise buildings which leverages DVAs to reduce the required self-weight of WLSS in meeting the critical code-specific occupant wind comfort criteria, leading to reduction in WLSS material utilization and, consequently, to the building embodied carbon. The framework relies on a novel bi-objective constrained optimization problem formulation which couples structural sizing optimization for minimum-weight WLSS (objective 1), with optimally tuned DVA having the smallest inertia property (objective 2) required for satisfying occupant comfort design criteria. Furthermore, a versatile numerical strategy is devised for the computationally efficient solution of the proposed optimization-driven design framework enabling the use of any type of the well-established WLSS sizing optimization algorithms in conjunction with any standard DVA tuning approach. Moreover, numerical application of the framework, supported by computationally efficient WLSS minimal-weight sizing and optimal DVA tuning algorithms, is considered to a routine 15-storey steel building equipped with a TMD and an IVA for exemplifying the applicability and usefulness of the framework. Note in passing that the herein developed framework follows the paradigm of optimal co-design systems approach, recently emerged in the field of wind renewable energy [41]. Note

further that some previous studies pursued structural weight reduction for the earthquake resistant design of buildings by introducing damping devices [42–44], which have been recently reviewed in Takewaki and Akehashi [45]. However, to the best of the authors' knowledge, this is the first time in the literature that DVAs are used within a systematic WLSS design framework to promote concurrently low-embodied carbon and resilience to wind hazard considerations in routine VS-sensitive high-rise buildings with a view to improve the sustainability of height-wise urban development.

The remainder of the paper is organised as follows. Section 2 discusses the background of the integrated design framework, defines the underlying optimization problem, and presents an efficient parallelizable numerical solution scheme. Sections 3 and 4 review an efficient discrete sizing optimization algorithm for minimum-weight WLSS design under a natural frequency constraint and an optimal DVA tuning approach for minimizing floor accelerations in wind-excited buildings, respectively. Section 5 presents an illustrative numerical application of the framework for a benchmark steel building and discusses numerical results and implications. Lastly, Section 6 summarizes concluding remarks.

2. Proposed Integrated Optimization-Driven Design Framework

2.1. Background and Practical Considerations. Tall buildings with height-to-width aspect ratios above 3 may be susceptible to excessive wind-borne oscillations in the crosswind direction (i.e., within the plane normal to the wind direction) due to VS-induced aerodynamic forces [3]. This is commonly the case for high-rise buildings with a relatively flexible WLSS whose natural frequency of the dominant sway vibration mode, f_1, is lower than 1 Hz [46]. Indeed, in such structures, even under moderate wind actions, the likelihood of f_1 resonating with the frequency of VS-induced forces is high [4]. This is demonstrated by the typical crosswind force power spectra plotted in Figure 1(a) at different floors for the 15-storey case-study building, examined later in the illustrative numerical application, under a random wind field with 20 m/s reference mean wind velocity. Combined with the low inherent damping of slender buildings, these aerodynamic forces may produce excessive horizontal floor accelerations, $\max\{\ddot{\mathbf{x}}_{\text{floor}}\}$, causing occupant discomfort and, ultimately, vibration serviceability failure, as human motion perception is sensitive to accelerations [5]. To this end, building design regulations safeguard vibration serviceability by specifying a floor acceleration threshold, $\ddot{x}_{\text{thres}}$, not to be exceeded under a nominal site-specific design wind velocity (e.g., [6, 7]). This threshold reduces as f_1 increases [5] so that the crosswind serviceability design criterion can be mathematically written as

$$\max\{\ddot{\mathbf{x}}_{\text{floor}}(\mathbf{a})\} \leq \ddot{x}_{\text{thres}} \propto f_1(\mathbf{a})^{-\theta}, \tag{1}$$

where θ is a positive number. In (1), the dependence of $\max\{\ddot{\mathbf{x}}_{\text{floor}}\}$ and of f_1 on the stiffness of the WLSS is explicitly expressed by means of the vector $\mathbf{a}$ collecting the sizes (i.e., cross-sectional areas) of the structural members in the WLSS.

In typical VS-sensitive high-rise buildings, the crosswind serviceability criterion in (1) is more critical in the design of the WLSS than the ultimate and serviceability limit state criteria in the along-wind direction [18]. In the current state of practice, the criterion in (1) is commonly met in routine VS-sensitive buildings by increasing the lateral stiffness of the WLSS, which typically involves increasing the number and/or the size of WLSS's structural members (e.g., [32]). Notably, this approach is in principle cost-ineffective as the comfort criterion in equation (1) becomes more stringent (i.e., $\ddot{x}_{\text{thres}}$ reduces) as frequency f_1 increases. Still, the rate of reduction of $\ddot{x}_{\text{thres}}$ with f_1 is slower compared to the rate of reduction of $\max\{\ddot{\mathbf{x}}_{\text{floor}}\}$ with f_1. This is because the VS forces exerted on the structure attenuate swiftly as f_1 departs from the VS frequency and, thus, from the frequency band where vibration serviceability check is commonly critical (usually 0.1 Hz to 1 Hz) as indicated in Figure 1(a) [47]. Hence, upon sufficient WLSS stiffening, the condition in equation (1) can be met as graphically seen in Figure 1(b). Nevertheless, this comes at the cost of increasing structural material usage in the WLSS as exemplified in Figure 1(c), which plots the WLSS self-weight, $M(\mathbf{a})$, of the case-study steel building considered in the illustrative example as a function of f_1.

In this context, the required WLSS member sizes to meet the criterion in (1) gradually increase for taller and taller buildings, becoming, eventually, economically prohibitive. To this end, DVAs with inertial property, m_{DVA}, are employed to facilitate meeting (1) in several landmark tall buildings [19, 20]. This is achieved by optimally tuning the stiffness and damping properties of the DVA, denoted by k_{DVA} and c_{DVA}, respectively, for a given f_1 (i.e., given a WLSS with member sizes $\mathbf{a}$). In this setting, the higher the inertial m_{DVA} property is, the more effective the DVA becomes in mitigating VS-induced floor accelerations, at the expense of higher DVA upfront cost which typically increases with m_{DVA} [48]. In this respect, DVAs with sufficiently large m_{DVA} (i.e., secondary mass for TMDs or inertance for IVAs) are used as a retrofit measure to satisfy serviceability occupant comfort design criteria (e.g., [8, 24]).

Motivated by the potential of DVAs to mitigate the critical crosswind floor accelerations in tall buildings, a novel design framework for routine VS-sensitive high-rise buildings is herein put forward aiming to achieve minimum-weight WLSS by optimally sizing the WLSS structural members together with the optimal DVA tuning in meeting the critical serviceability criterion in (1). Importantly, the proposed framework treats the DVA as an integrated part of the WLSS in an optimization-driven design context rather than as an appendage used for retrofitting a code-deficient WLSS. This innovative design approach for VS-sensitive high-rise buildings is underpinned by the optimal design problem formulation discussed in the next section.

2.2. Novel Integrated Bi-Objective Optimal Design Problem Formulation. To leverage the potential of the DVA for minimizing the required structural material in the WLSS, the

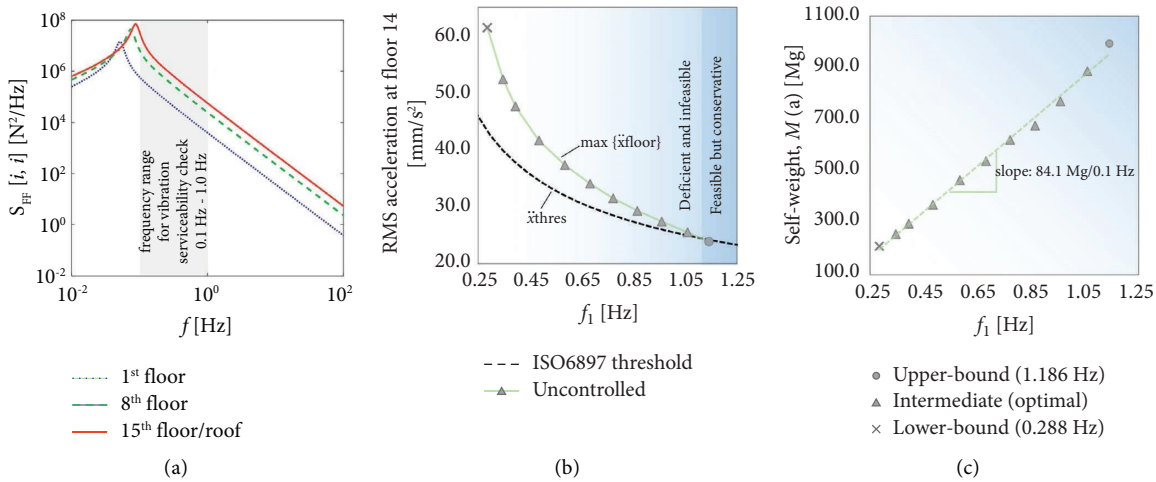

FIGURE 1: (a) Power spectra of design crosswind forces for the case-study building in Figure 3(a), based on the model by Liang et al. [3] (see Appendix A), (b) root mean square 14th floor acceleration of the case-study building in Figure 3(a) for optimally sized WLSSs with different f_1 frequencies versus ISO6897 [6] occupant comfort threshold, and (c) self-weight of the optimally sized WLSSs versus f_1 frequency.

developed framework pursues the optimal sizing of the WLSS members in **a** together with the optimal tuning of the DVA. The latter should have sufficient inertia m_{DVA} to satisfy the floor acceleration serviceability constraint $\ddot{x}_{\mathrm{thres}}$. The need for integrating WLSS optimal sizing for minimum self-weight M (**a**) with DVA optimal tuning stems from the fact that $\ddot{x}_{\mathrm{thres}}$ and DVA tuning depend on the fundamental natural frequency, f_1, of the uncontrolled WLSS, which, in turn, depends on **a**, as previously discussed. In this setting, a minimum-weight design problem is mathematically expressed by the following novel constrained optimization problem:

$$\begin{aligned}&\min\left\{M(\mathbf{a}), m_{\mathrm{DVA}}\right\},\\ &\text{such that: } \max\left\{\ddot{\mathbf{x}}_{\mathrm{floor}}(\mathbf{a},\mathbf{y},m_{\mathrm{DVA}})\right\}-\ddot{x}_{\mathrm{thres}}(f_1(\mathbf{a}))\le 0,\\ &\text{for } \mathbf{a}^{\min}\le\mathbf{a}\le\mathbf{a}^{\max} \text{ and } \mathbf{y}^{\min}\le\mathbf{y}=[k_{\mathrm{DVA}},c_{\mathrm{DVA}}]\le\mathbf{y}^{\max}.\end{aligned} \tag{2}$$

The design variables (DVs) in the above optimization problem are the cross-sectional areas of the WLSS members in vector **a** (structural DVs) and the DVA stiffness, k_{DVA}, and damping, c_{DVA} (control DVs), in vector **y**. The DVs are side-constrained by the lower-bound values in vectors $\mathbf{a}^{\min}$ and $\mathbf{y}^{\min}$ and by the upper-bound values in vectors $\mathbf{a}^{\max}$ and $\mathbf{y}^{\max}$ as indicated in (2). These side constraints are application-dependent, specified based on practical considerations discussed in later sections. Furthermore, the optimization problem in (2) comprises two upfront cost-related objectives to be concurrently minimized: the total self-weight of the WLSS, M(**a**), and the DVA inertial property, m_{DVA} (either secondary mass for TMDs or inertance for IVAs). Some discussion on the choice of the above two objectives is given in the following.

For steel and mass timber structures, the self-weight M(**a**) is proportional to both the monetary structural material cost and the environmental impact in terms of embodied CO_2 of the WLSS (e.g., [49]). Therefore, adopting the self-weight M(**a**) as an objective function in (2) is directly applicable for minimizing upfront WLSS material cost and environmental impact in VS-sensitive steel and mass timber high-rise buildings. For reinforced concrete WLSSs, the stiffness and mass properties of individual members, relevant to the considered optimal sizing with a frequency constraint assuming elastic behaviour, stem from the outer dimensions of members as reinforcing steel bars have insignificant contribution to the elastic lateral stiffness of the WLSS. Accordingly, the self-weight of concrete is accounted for in the self-weight M(**a**) calculation in (2), while structural DVs become, for instance, sectional widths and depths of concrete members (e.g., [50]). In this regard, the formulation in (2) minimizes only the share of concrete in the upfront cost and environmental impact of the WLSS, and not the overall WLSS costs strictly as commonly pursued in the literature (e.g., [51, 52]). In any case, if desired, the contribution of steel reinforcement can be considered in the self-weight evaluation by introducing a reinforcement ratio (defined as the ratio between the area of rebars to the effective area of the section) to each design group of concrete members. For composite WLSSs (e.g., steel-concrete, steel-timber, and so on), the weight of different materials/members contributing to the stiffness and mass of the WLSS need to be aggregated in calculating M(**a**), while the structural DVs may involve the cross-sectional area or other appropriate sectional properties of different materials for the same structural member. To this end, solving (2) may neither lead to optimality in terms of construction cost, nor to optimality in terms of environmental impact. To this aim, additional material/structure-specific information related to the monetary cost and embodied carbon emission may need to be imposed to achieve minimization of either of the two costs [53], though such considerations lie beyond the scope of this work. Irrespective of the WLSS material,

note that only cross-sectional areas of members are herein selected as structural DVs. This consideration facilitates the weight-minimal design formulation in (2) and can be supported by expressing all other sectional properties contributing to the WLSS stiffness in terms of the cross-sectional area (see, e.g., Appendix B for an example pertaining to a typical steel WLSS).

To support the choice of m_{DVA} as the second objective function to minimize in (2), it is noted that the secondary mass is proportional to the upfront cost of commercial TMDs [48] typically installed on top floor of tall buildings for wind vibration mitigation. Thus, taking m_{DVA} to be the secondary mass for TMDs in the objective function of (2) minimizes the upfront TMD cost. Moreover, this choice is consistent with the minimization of M (a) in pursuit of a self-weight minimal design for the DVA-equipped WLSS. For the case of IVAs, whose vibration mitigation effectiveness relies on the inertance property endowed by inerter devices (e.g., [22, 26–28]), m_{DVA} in (2) becomes the inertance of the IVA, such that the design problem in (2) seeks to minimize the inertance. This choice relies on the fact that in the most widely studied IVAs for motion control of buildings under lateral loads, an increase in inertance leads to increasing forces developed in the inerter device and transferred to the host structure (see, e.g., [24, 54]). In this regard, while scaling up the inertance property does not lead to significant increase of inerter device weight (e.g., [29, 55, 56]), the upfront cost of IVAs with higher inertance may be higher in practice as special device and connection designs will be required to accommodate the larger control forces. In this respect, minimizing the inertance in the design problem of (2) translates directly into upfront IVA cost minimization.

2.3. Efficient Solution Strategy of the Integrated Optimal Design Problem. The optimization problem in (2) is non-trivial to solve. Notwithstanding the potentially large number of structural DVs involved (i.e., member sizes in $\mathbf{a}$), both f_1 and $\ddot{x}_{\mathrm{thres}}$, which govern the optimal DVA tuning and required m_{DVA}, respectively, depend heavily on the member sizes. Furthermore, the same holds for $\max\{\ddot{\mathbf{x}}_{\mathrm{floor}}\}$ whose evaluation requires explicit structural dynamic analysis of the DVA-equipped WLSS for the design wind load which can be computationally intensive. Nevertheless, there exist a plethora of efficient member sizing optimization approaches for WLSSs made of different materials with no control devices (e.g., [32, 33, 49, 50, 57]), as well as efficient optimization algorithms for the optimal DVA tuning for a given WLSS (e.g., [21, 24]). In this regard, a three-stage solution strategy to (2) is herein proposed to decouple the optimal WLSS sizing problem from the optimal DVA tuning problem, thus enabling the employment of existing algorithms to solve each of the two problems independently.

The first stage involves member sizing to minimize WLSS weight, M ($\mathbf{a}$), for prespecified target frequencies, f_{target}. Stage two involves optimal DVA tuning for prespecified m_{DVA} values aiming to minimize floor accelerations in the minimum-weight WLSSs obtained from stage one under the design crosswind load. Stage three assesses the performance of the optimized DVA-equipped WLSS with $f_1 = f_{\mathrm{target}}$ frequency against the codified threshold $\ddot{x}_{\mathrm{thres}}$. By considering multiple f_{target} and m_{DVA} values, a set of optimal integrated DVA-plus-WLSS designs is determined which all satisfy the crosswind serviceability criterion in (1). This set of solutions quantifies the trade-off between the two objectives in (2), i.e., $M(\mathbf{a})$ and m_{DVA}, thereby representing a Pareto front of non-dominant designs whose $M(\mathbf{a})$ cannot be further reduced without increasing m_{DVA} and vice versa. Ultimately, the design engineer can choose one solution from the Pareto optimal set based on various practical considerations including DVA cost and desired savings in WLSS material usage and embodied carbon footprint.

The flowchart of the proposed solution strategy to the bi-objective optimization problem in (2) is delineated in Figure 2. According to it, the range of f_{target} frequencies is specified in the initialization step, given a fixed WLSS layout, design crosswind loads, and the crosswind occupant comfort serviceability criterion. The lowest target frequency value, ${f_{\mathrm{target}}}^{\min}$, corresponds to a WLSS designed to meet all serviceability and ultimate limit state design criteria for gravitational and (static) along-wind loads, using standard structural design methods. The member sectional sizes of this design become the lower boundary of the side constraint on structural DVs, i.e., $\mathbf{a}^{\min}$. For a wind-sensitive building, this design will not meet the crosswind serviceability criterion. Thus, one more WLSS design is further performed in which the WLSS is sufficiently stiffened to satisfy the crosswind serviceability criterion in (1) without the use of a DVA. This may be achieved using either conventional trial-and-error or automated optimization-based approaches previously discussed. Regardless of the approach used, the latter design will always have a higher fundamental natural frequency than ${f_{\mathrm{target}}}^{\min}$. This frequency becomes the highest target frequency value, ${f_{\mathrm{target}}}^{\max}$, and the corresponding member sectional sizes become the upper boundary of the side constraint on structural DVs, i.e., $\mathbf{a}^{\max}$.

These target frequencies can be made equally spaced at $\Delta f = ({f_{\mathrm{target}}}^{\max} - {f_{\mathrm{target}}}^{\min})/(j-1)$. Clearly, a higher number of WLSS designs increases the resolution of the Pareto optimal solutions (from which a single integrated design can be chosen) at the expense of higher computational cost. In the subsequent optimal DVA tuning stage, a set of k optimal DVA tunings is performed for each of the j minimal-weight WLSS designs with respect to the crosswind serviceability criterion obtained in previous steps (note that the one with ${f_{\mathrm{target}}}^{\max}$ is code-compliant). Each DVA tuning aims to determine the control DVs in $\mathbf{y}$ vector to minimize the maximum floor acceleration (usually attained at the highest occupied floor) under the design crosswind excitation for a given inertial value, m_{DVA}. Overall, k m_{DVA} values, possibly equally spaced or otherwise, are considered within an interval $[{m_{\mathrm{DVA}}}^{\min}, {m_{\mathrm{DVA}}}^{\max}]$. The value of ${m_{\mathrm{DVA}}}^{\min}$ may be set to zero to signify the uncontrolled WLSS cases. Furthermore, the upper-bound value of ${m_{\mathrm{DVA}}}^{\max}$ is DVA-dependent and is defined as the minimum DVA inertia required for the WLSS with the lowest natural frequency, ${f_{\mathrm{target}}}^{\min}$ (corresponding to the $\mathbf{a}^{\min}$ side constraint), to meet the serviceability design criterion of (1). The

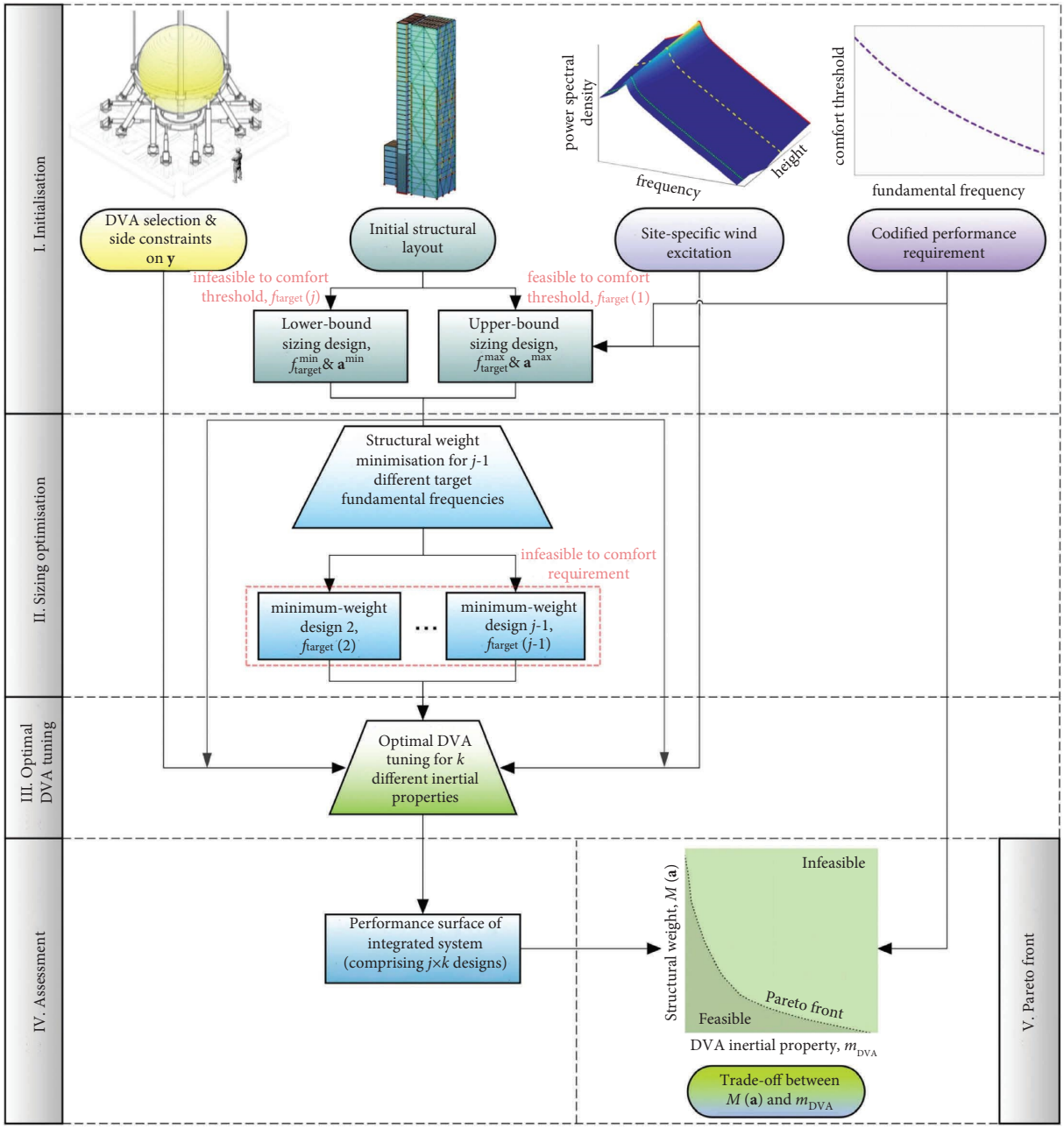

FIGURE 2: Flowchart of novel framework for minimal-weight design of inertial DVA-equipped tall buildings to meet wind-related dynamic serviceability criteria.

performance of the $j \times k$ different DVA-equipped WLSSs in terms of $\max\{\ddot{\mathbf{x}}_{floor}\}$ under the design crosswind loading can be plotted on the $f_1(\mathbf{a})$-m_{DVA} plane or, alternatively, on the two-objective $M(\mathbf{a})$-m_{DVA} plane to derive numerically a performance surface. The intersection of the performance surface with the $\ddot{x}_{thres}$ curve provides Pareto optimal solutions of (2). If needed, these solutions can be refined by repeating the optimal sizing and optimal tuning stages for a set of $f_1(\mathbf{a})$-m_{DVA} pairs found upon interpolation of the performance surface with the $\ddot{x}_{thres}$ design curve. In this regard, if $m_{DVA}{}^{max}$ is too large or too expensive to be adopted in design, then lower m_{DVA} values can be adopted chosen from the Pareto optimal front of solutions which will correspond to a heavier WLSS. Therefore, the proposed framework supports versatile and practical decision making for design engineers in view of total upfront cost considerations.

The applicability of the proposed integrated design optimization framework is numerically illustrated in Section 5, for which a numerical implementation of the solution strategy is required. To this aim, the following two sections detail the formulations and algorithmic solutions adopted for the numerical illustration of the framework. First, an optimality-criteria (OC)-based algorithm is presented for sizing optimization of a WLSS under a frequency constraint (Section 3), and then a numerical pattern search method is

outlined for optimal DVA tuning (Section 4). It is noted, however, that alternative algorithms and approaches can be adopted for the numerical implementation of the framework, while the solution strategy can be expedited by fully parallelizing the j-1 optimal sizing designs and the k optimal tunings for each j WLSS.

3. Optimality-Criteria-Based Member Sizing under a Frequency Constraint

3.1. Formulation of Optimality-Criteria Design Optimization Problem. An efficient formulation is adopted in this work to address the minimum-weight WLSS member sizing problem for any target fundamental natural frequency, f_{target}, required in the proposed solution strategy in Figure 2, relying on an OC-based algorithm originated in the early work of Venkayya [58, 59]. For a WLSS comprising S structural members, the minimum-weight sizing problem can be mathematically expressed as

$$\min_{\mathbf{a}} \left\{ M(\mathbf{a}) = \sum_{s=1}^{S} \rho_s l_s a_s \right\}, \tag{3}$$

subjected to the side constraint $\mathbf{a}^{\min} \le \mathbf{a} \le \mathbf{a}^{\max}$ and to the frequency constraint

$$f_1(\mathbf{a}) - f_{\text{target}} = 0. \tag{4}$$

In (3), ρ_s, l_s, and a_s ($s = 1,\ldots,S$) are the material density, the length, and the cross-sectional area of structural member s, respectively. Note that grouping of structural members through equal size constraints can be readily imposed in (3) in support of buildability, practicality, and cost-efficiency, as commonly considered in optimal member sizing. This consideration results in having N number of active structural DVs (cross-sectional areas) in vector $\mathbf{a}$ with $N \le S$.

Assuming continuous-valued DVs in $\mathbf{a}$, the solution of the optimal sizing problem is pursued by firstly formulating the Lagrangian function by adjoining the objective function in (3) with the frequency constraint in (4) through the unknown Lagrange multiplier λ as

$$L(\mathbf{a}, \lambda) = M(\mathbf{a}) - \lambda \left[f_1(\mathbf{a}) - f_{\text{target}} \right]. \tag{5}$$

Then, the problem in (3) can be solved by finding the stationary point of $L(\mathbf{a}, \lambda)$ with respect to all the n elements of $\mathbf{a}$ (i.e., the point at which the first derivative of $L(\mathbf{a}, \lambda)$ with respect to $\mathbf{a}$ is zero) through the solution of the following N system of equations:

$$\frac{\lambda}{\rho_n l_n} \frac{\partial f_1(\mathbf{a})}{\partial a_n} = 1 \, (n = 1, N). \tag{6}$$

The last system of equations defines the OC which need to be simultaneously satisfied by structural DVs $\mathbf{a}$ to reach a frequency-constrained minimum-weight WLSS. Furthermore, it is readily seen that the first-order derivative test of $L(\mathbf{a}, \lambda)$ with respect to λ yields the frequency constraint in (4). In this regime, (4) and (6) define a system of N+1 coupled equations for N+1 unknowns, namely, the N active structural DVs in $\mathbf{a}$ plus the λ multiplier. An efficient iterative algorithm is presented next for solving the above $N+1$ system of equations.

3.2. Iterative Resizing Algorithm for Solving the Optimality-Criteria Problem. The optimization problem in (3) subjected to the constraint in (4) is strictly convex [60]. Therefore, for a sufficiently wide range $[\mathbf{a}^{\min}, \mathbf{a}^{\max}]$, there always exists a single global optimum design (stationary) point, $\mathbf{a}^{\text{opt}}$, at which the OC in (6) hold [61]. In this setting, a numerical algorithm is herein adopted to iteratively update the active structural DVs using the OC in (6) towards $\mathbf{a}^{\text{opt}}$ where the target frequency constraint $f_1 = f_{\text{target}}$ is satisfied by the WLSS with minimum self-weight $M(\mathbf{a}^{\text{opt}})$. To this aim, a linear recursive relation derived directly from (6) is used, written for the n-th active DV at the p-th iteration as [57]

$$a_n^{(p+1)} = \left\{ 1 + \frac{1}{\eta} \left[\frac{\lambda^{(p)}}{\rho_n l_n} \left(\frac{\partial f_1(\mathbf{a})}{\partial a_n} \right)^{(p)} - 1 \right] \right\} a_n^{(p)} \, (n = 1, N). \tag{7}$$

In the last equation, the relaxation parameter η controls the convergence rate of the DVs: as η becomes smaller, the value of $a_n^{(p)}$ is scaled (updated) to a larger extent, and vice versa. Furthermore, an expression for the Lagrangian multiplier at iteration p, $\lambda^{(p)}$, appearing in (7) can be reached by first writing the change in the fundamental frequency between two consecutive iterations using a first-order Taylor series expansion approximation about the DVs as

$$f_1^{(p+1)} - f_1^{(p)} = \sum_{n=1}^{N} \left(\frac{\partial f_1}{\partial a_n} \right)^{(p)} \left(a_n^{(p+1)} - a_n^{(p)} \right), \tag{8}$$

and, then, by substituting (7) into (8), which yields

$$\lambda^{(p)} = \frac{\sum_{n=1}^{N} \left(\partial f_1 / \partial a_n \right)^{(p)} a_n^{(p)} + \eta \left(f_{\text{target}} - f_1^{(p)} \right)}{\sum_{n=1}^{N} \left[\left(\partial f_1 / \partial a_n \right)^{(p)} \right]^2 a_n^{(p)} / \rho_n l_n}. \tag{9}$$

The latter expression has been derived by assuming that the frequency constraint in (4) is satisfied after p iterations, that is, $f_1^{(p+1)} = f_{target}$.

In this context, (7) and (9) can be used iteratively to solve (3) and (4). To this end, an economical calculation of the partial derivatives $(\partial f_1 / \partial a_n)^{(p)}$ is required for the efficient numerical implementation of (7) and (9). Assuming that the WLSS is modelled using the standard linear finite element method, the partial derivatives can be efficiently approximated by the expression [62]

$$\left(\frac{\partial f_1}{\partial a_n} \right)^{(p)} = \frac{1}{4\pi \sqrt{\boldsymbol{\varphi}_1^T \mathbf{K}_s(\mathbf{a})^{(p)} \boldsymbol{\varphi}_1}} \left(\boldsymbol{\varphi}_1^T \left(\frac{\partial \mathbf{K}_s(\mathbf{a})}{\partial a_n} \right)^{(p)} \boldsymbol{\varphi}_1 \right) (n = 1, \ldots, N), \tag{10}$$

in which $\mathbf{K}_s(\mathbf{a})^{(p)}$ is WLSS stiffness matrix at the p-th iteration and the superscript "T" denotes matrix transposition. In (10), the mode shape is normalized such that $\boldsymbol{\varphi}_1^{\mathrm{T}} \mathbf{M}_s \boldsymbol{\varphi}_1 = 1$ with $\mathbf{M}_s$ being the mass matrix accounting for the nominal dead and live loads of the building. Furthermore, $\boldsymbol{\varphi}_1$ is taken as independent of changes to member

sizes $\mathbf{a}$ at any iterative step, which is a usual assumption to achieve computational efficiency in calculating the derivatives $(\partial f_1/\partial a_n)^{(p)}$ without significant loss of accuracy [62]. Moreover, the first derivative of the stiffness matrix in (10) may be approximated using the finite difference-based expression

$$\left(\frac{\partial \mathbf{K}_s}{\partial a_n}\right)^{(p)} = \frac{\mathbf{K}_s^{(p)} - \mathbf{K}_n^{(p-1)}}{a_n^{(p)} - a_n^{(p-1)}}, \tag{11}$$

where $\mathbf{K}_n{}^{(p-1)}$ is a perturbed stiffness matrix compared to $\mathbf{K}_s^{(p)}$ in which the element stiffness matrix for member n comes from the previous p-1 step.

At this juncture, it is important to note that the continuous-valued updating of the structural DVs through the iterative application of (7) and (9) is guaranteed to converge to the optimal solution of (3) and (4), provided that no side constraint is violated [58]. In this regard, (7) and (9) are iteratively implemented in a first pass without imposing the side constraints $\mathbf{a}^{\min} \le \mathbf{a} \le \mathbf{a}^{\max}$. Side constraints are checked after convergence of the first pass to a tentative $\mathbf{a}^{\text{opt*}}$. If one or more cross-sectional areas in $\mathbf{a}^{\text{opt*}}$ violate the side constraint(s), then they are removed from the vector $\mathbf{a}$ of the active DVs, and their values are set equal to the side constraint values that were violated. Next, (7) and (9) are iteratively re-executed for the same target frequency and for vector $\mathbf{a}$ with reduced number of structural DVs. The above steps are repeated until no side constraint is violated by any of the active DVs, at which stage the optimal cross-sectional properties of all groups of members have been obtained. Lastly, practically feasible member sizes are specified by mapping the obtained continuous-valued cross-sectional member properties onto a discrete set of possible section sizes comprising sections with rounded-up dimensions in reinforced concrete and timber structures (or structural members) or catalogues of commercially available sections for steel structures (or structural members).

In the illustrative example of Section 5 pertaining to a steel structure, in-house developed routines hard-coded in MATLAB® are used to implement the herein presented OC-based optimal sizing algorithm with side-constraint verification and mapping of section properties to commercial steel sections. The routines include finite element code for automated stiffness matrix assembly and updating as well as modal analysis to find $\boldsymbol{\varphi}_1$.

4. Optimal Tuning of DVA for Minimizing Floor Acceleration

4.1. Formulation of the Optimal DVA Tuning Problem. With j-1 optimally sized WLSSs (for a set of j-1 prespecified f_{target} fundamental natural frequency values) having been determined, the solution strategy in Figure 2 proceeds with the optimal DVA tuning stage. As discussed in Section 2.3, the code-specific threshold $\ddot{x}_{\text{thres}}$ does not enter the optimal DVA tuning. Instead, the criterion in (1) is being checked for optimal DVA-equipped WLSSs at a subsequent stage to determine the minimum required DVA inertia property, m_{DVA}, that satisfies the threshold for each one of the j different WLSS. In this respect, the optimal DVA tuning stage aims to minimize the maximum crosswind floor acceleration response, $\max\{\ddot{\mathbf{x}}_{\text{floor}}\}$, under the design wind load for each j WLSS separately and for a set of k prespecified values of the DVA inertial property m_{DVA} within a range $[m_{\text{DVA}}{}^{\min}, m_{\text{DVA}}{}^{\max}]$. Thus, a total of $j{\times}k$ optimal DVA tunings are undertaken, each one seeking to determine optimal control DVs, namely, DVA stiffness, k_{DVA}, and DVA damping, c_{DVA}, that minimize $\max\{\ddot{\mathbf{x}}_{\text{floor}}\}$ given m_{DVA} and a WLSS with $\mathbf{a}^{\text{opt}}$ cross sections corresponding to some f_{target} value. The optimal DVA tuning problem is mathematically expressed as

$$\min_{\mathbf{y}} \left\{\max\left\{\ddot{\mathbf{x}}_{\text{floor}}\left(\mathbf{y} \mid \mathbf{a}^{\text{opt}}, m_{\text{DVA}}\right)\right\}\right\}, \tag{12}$$

subjected to the side constraint $\mathbf{y}^{\min} \le \mathbf{y} \le \mathbf{y}^{\max}$. Commonly, the two control DVs, collected in the vector $\mathbf{y}$, are expressed by the dimensionless DVA frequency and damping ratios defined as

$$\nu_{\text{DVA}} = \frac{\sqrt{k_{\text{DVA}}/m_{\text{DVA}}}}{2\pi f_{\text{target}}} \text{ and } \xi_{\text{DVA}} = \frac{c_{\text{DVA}}}{2\sqrt{k_{\text{DVA}} m_{\text{DVA}}}}, \tag{13}$$

respectively, which facilitates the specification of physically meaningful side constraints $\mathbf{y}^{\min}$ and $\mathbf{y}^{\max}$ and further supports an efficient numerical solution of (12) as discussed in the following section. Once optimal values for the dimensionless ratios, ν_{DVA} and ξ_{DVA}, are determined, the optimal values of DVA stiffness, k_{DVA}, and damping, c_{DVA}, are readily found from (13).

4.2. Numerical Solution of the Optimal Tuning Problem. The evaluation of the objective function, $\max\{\ddot{\mathbf{x}}_{\text{floor}}\}$, in (12) requires the structural analysis of the DVA-equipped WLSS for the nominal design wind loading, and therefore, the gradient of $\max\{\ddot{\mathbf{x}}_{\text{floor}}\}$ cannot be generally (or at least efficiently) found or approximated (semi-) analytically. In this regard, non-gradient optimization algorithms can be used to solve numerically (13) (e.g., [63, 64]). In the numerical part of this work, the efficient algorithm developed in [24, 25] and hard-coded in MATLAB® is used for the task. The adopted algorithm applies standard pattern search [63] iteratively with progressively narrower search range in $\mathbf{y}$ by "zooming-in" the neighbourhood of the optimal ν_{DVA} and ξ_{DVA} values found in the previous iteration, to expedite the solution process. The stoppage criterion for the iterations checks the absolute difference of successive $\max\{\ddot{\mathbf{x}}_{\text{floor}}\}$ against a prespecified convergence tolerance [25]. In the illustrative numerical example (Section 5), the initial search range is taken as $\mathbf{y}^{\min} = [0.5, 0.0]$ and $\mathbf{y}^{\max} = [1.5, 1.0]$ with convergence tolerance set to 1E-2.

The efficient numerical solution of the optimal DVA tuning is herein further facilitated by undertaking frequency-domain random vibration structural analysis to evaluate $\max\{\ddot{\mathbf{x}}_{\text{floor}}\}$. Conveniently, such analysis is supported by representing the design wind load as a stationary random field defined by a power spectral density matrix (PSDM) $\mathbf{S}_{\mathbf{FF}}(\omega)$ in the domain of circular frequencies ω, which is quite common in practice (see [4] and Appendix A).

Typically, only a small number of dynamic degrees of freedom (DOFs) need to be accounted for in the analysis, corresponding to lateral translational displacements for each building floor plus the displacement of the DVA. To this end, reduced order dynamical modelling of the DVA-equipped WLSS may be employed to define a low-order stiffness matrix $\mathbf{K}_{\text{low}}$ containing only the dynamic DOFs. The latter matrix can be derived from the full $\mathbf{K_s}$ matrix either by static condensation (e.g., [25]) or by back-solving the modal analysis equations using a mass matrix containing only the dynamic DOFs (e.g., [24]). In this regime, $\max\{\ddot{\mathbf{x}}_{\text{floor}}\}$ can be efficiently computed by first obtaining the response acceleration PSDM of the low-order dynamical system as

$$\mathbf{S}_{\ddot{\mathbf{x}}\ddot{\mathbf{x}}}(\omega) = \omega^4 \mathbf{B}(\omega)^* \mathbf{S}^+_{\mathbf{FF}}(\omega) \mathbf{B}(\omega), \tag{14}$$

where $\mathbf{S}^+_{\mathbf{FF}}(\omega)$ is an augmented excitation PSDM with additional zero rows and columns corresponding to the DOF of the DVA which is not externally excited by the wind, the superscript " $*$ " denotes complex conjugation, and

$$\mathbf{B}(\omega) = \left(\mathbf{K}_{\text{low}} - \omega^2 \mathbf{M}_{\text{low}} + i\omega \mathbf{C}_{\text{low}}\right)^{-1}. \tag{15}$$

In the last equation, $\mathbf{M}_{\text{low}}$ and $\mathbf{C}_{\text{low}}$ are the mass and damping matrices of the low-order dynamic system, $i = \sqrt{-1}$, and the superscript "−1" denotes matrix inversion. Then, the root mean square (RMS) acceleration response of the q-th floor is obtained as

$$\sigma_{\ddot{x}_q} = \sqrt{\int_0^{\omega_{\max}} \mathbf{S}_{\ddot{\mathbf{x}}\ddot{\mathbf{x}}}[q,q]\,\mathrm{d}\omega}, \tag{16}$$

by integrating the main diagonal element (q,q) of the response acceleration PSDM in (14) on the frequency axis up to a maximum (cutoff) frequency $\omega_{\max}$ above which the energy of the underlying stochastic response processes is negligible. Any standard quadrature rule can be used to calculate the integral in (16). In the numerical part of this work, the trapezoidal rule as implemented by the MATLAB built-in function "trapz" is used for the task. Ultimately, the $\max\{\ddot{\mathbf{x}}_{\text{floor}}\}$ objective function in (12) can be taken as the largest RMS response acceleration value from all the q building floors in (16).

Note in passing that in case the code-specific floor acceleration threshold, $\ddot{x}_{\text{thres}}$, is defined in terms of the RMS value, then (16) can also be used for the assessment stage of the flowchart in Figure 2. Nevertheless, if $\ddot{x}_{\text{thres}}$ is defined in terms of the peak value, then the RMS value in (16) needs to be multiplied by a semi-empirical peak factor (see, e.g., [4]). As a final remark, in the less common case that the design crosswind loading is given in time domain (e.g., time series from direct wind tunnel testing), then computationally demanding response history analysis needs to be undertaken to evaluate $\max\{\ddot{\mathbf{x}}_{\text{floor}}\}$ and to assess the DVA-equipped WLSS against the $\ddot{x}_{\text{thres}}$.

5. Illustrative Numerical Application

5.1. Case-Study Building Description and Initial Uncontrolled WLSS Designs. To illustrate the applicability of the integrated design framework and solution strategy presented in Section 2, the doubly symmetric, 15-storey, steel moment-resisting frame (MRF) building shown in Figure 3(a) is taken as case study of a routine wind-sensitive high-rise building. The total building height is 49.8 m (ground floor is 5 m high and typical floor is 3.2 m high). The WLSS comprises 4 parallel, 3-bay MRFs along two horizontal perpendicular axes with all beam-to-column connections taken as rigid. Floor slabs are assumed to act as rigid diaphragms in their plane and gravitational design loads are uniformly distributed. Columns are taken to have (welded) square hollow sections (SHS), while (standard) Universal Beams (UB) sections are used for beams. The practicality of the sizing design of the WLSS is supported by considering 5 member design groups with common cross-sectional sizes per every three storeys, namely, the perimetric beam, inner beam, central column, corner column, and perimetric column, as shown in Figure 3(b). Overall, 10 groups of beams and 15 groups of columns are considered in the WLSS sizing optimization, totalling 25 structural DVs. Note that due to the double symmetry along two perpendicular horizontal (principal) axes, the WLSS has two translational uncoupled vibration modes along the principal axes with the same natural frequency. This common natural frequency is the lowest, f_1, which dominates the acceleration response of the case-study structure to lateral (dynamic wind) loads for the occupant comfort consideration.

In order to find the lower-bound WLSS design and $f_{\text{target}}^{\min}$ for the sizing optimization (see Section 2), the WLSS of the case-study building is designed (using conventional trial-and-error design method) to meet all serviceability and ultimate limit state requirements according to Eurocode 3 [65], involving appropriate gravitational and static along-wind forces with a reference design wind speed $v_b = 20$ m/s (i.e., 10 min mean wind velocity at 10 m height assuming open flat terrain). The cross sections of 25 WLSS member groups of this design are reported in Table 1 (see also Table 3 in Appendix B for detailed section properties specification). This initial design has a self-weight of 209.3 Mg and a fundamental natural frequency of 0.288 Hz obtained by application of standard modal analysis to the detailed finite element model of the WLSS modelled using linear Timoshenko beams.

Further, the dynamic crosswind forces for assessing the case-study building's occupant comfort performance are represented by the spatially correlated stationary random field model of Liang et al. [3] is assumed for rough/urban terrain. For this wind profile, the crosswind force PSDM surface is plotted in Figure 3(c) as a continuous function of the elevation and excitation frequency. In the latter plot, the dominant VS frequency is clearly seen as a ridge on the PSDM surface, and the force magnitude increases with elevation (see also cross sections of the force PSDM surface at three different floors/elevations in Figure 1(a)). The ISO6897 : 1984 guideline [6] is adopted to define the crosswind occupant comfort (serviceability) design criterion, specified by the maximum floor acceleration given as

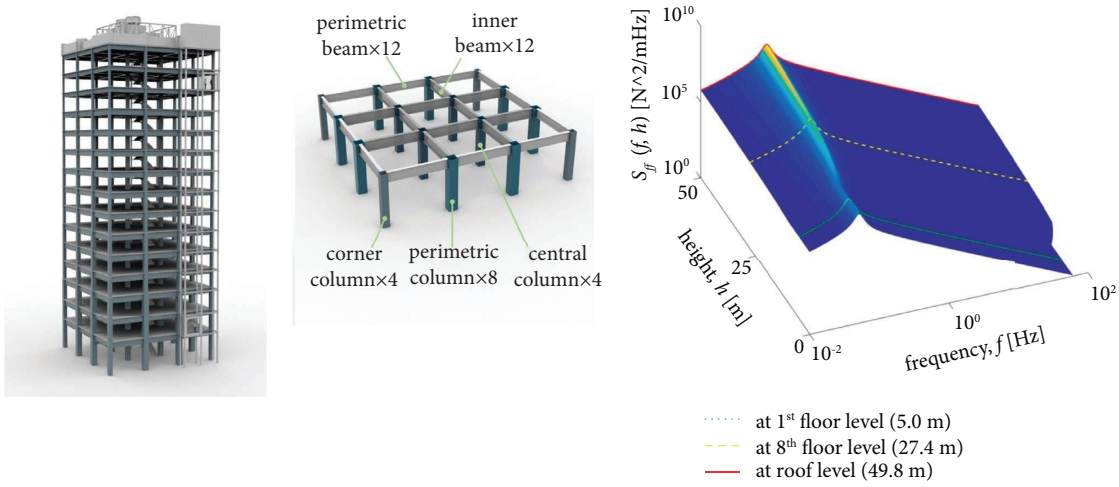

Figure 3: (a) 15-storey case-study building, (b) member design groups for sizing optimization of the case-study building's WLSS, and (c) power spectral density function of crosswind design forces for the case-study building.

Table 1: Cross sections of the lower-bound WLSS design of the case-study building.

Floor number	Lower-bound optimal design $f_1 = 0.288$ Hz, self-weight = 209.3 Mg				
	Groups of beams (standard UB)		Groups of columns (welded SHS)		
	Inner	Perimetric	Central	Corner	Perimetric
1–3	UB457 × 152 × 74	UB457 × 152 × 52	w400 *t*20	w280 *t*14	w360 *t*18
4–6	UB406 × 178 × 60	UB406 × 178 × 60	w320 *t*16	w280 *t*14	w320 *t*16
7–9	UB356 × 171 × 67	UB406 × 140 × 46	w280 *t*14	w200 *t*10	w280 *t*14
10–12	UB356 × 171 × 45	UB356 × 171 × 45	w240 *t*12	w160 *t*8	w240 *t*12
13–15	UB406 × 140 × 39	UB305 × 165 × 54	w200 *t*10	w160 *t*8	w200 *t*10

$$\ddot{x}_{\text{thres}} = \exp\left(-3.65 - 0.41 \ln f_1(\mathbf{a})\right), \tag{17}$$

in terms of RMS value and plotted in Figure 1(b) (broken line).

Due to the double symmetry of the case-study building, assessment against the crosswind serviceability criterion in (17) for the design crosswind forces in Figure 3(b) can be undertaken along any of the two structural principal axes. To this aim, frequency-domain random vibration analysis discussed in Section 4.2 is applied to a planar low-order dynamic model of the WLSS with only 15 translational DOFs (i.e., one per floor), derived in Appendix C. It is numerically found that the WLSS crosswind acceleration response is dominated by the first vibration mode and the maximum RMS floor acceleration is attained at the 14th (highest occupied) floor. This RMS acceleration value is much larger than the threshold value in equation (17) (point indicated with "$\ddot{x}_{\text{thresh}}$" in Figure 1(b)). Thus, the WLSS design in Table 1 does not satisfy the crosswind serviceability criterion, and the case-study building is indeed VS-sensitive and governed by the occupant comfort requirement. Therefore, this design is set as the "lower-bound" design according to the design flowchart in Figure 2, with $f_{\text{target}}{}^{\min} = 0.288$ Hz and with side constraints $\mathbf{a}^{\min}$ for the structural DVs equal to the cross-sectional properties in Table 1.

To this end, a second WLSS design is undertaken to satisfy the criterion in equation (17) through stiffening, using heavier steel sections. This is achieved for a WLSS with $f_1 = 1.186$ Hz for which the maximum RMS floor acceleration (at the 14th floor) under the design crosswind forces, obtained using (16) for the low-order 15-DOF system in Appendix C, equals the threshold value in (17) (point indicated by a filled circle in Figure 1(b)). This WLSS is designed using the sizing optimization algorithm in Section 3 with cross sections reported in Table 2. Being stiffer and thus stronger than the original WLSS design in Table 2, it meets all the other Eurocode 3 [65] design verifications. Therefore, this second WLSS design is set as the "upper-bound" design, as per the flowchart in Figure 2, with $f_{\text{target}}{}^{\max} = 1.186$ Hz and with side constraints $\mathbf{a}^{\max}$ for the structural DVs equal to the cross-sectional properties in Table 2.

It is worth noting that the fundamental natural frequency $f_1 = 1.186$ Hz of the upper-bound minimum-weight WLSS design of Table 2 is consistent with field-measured natural frequencies of portfolios of actual steel MRF buildings with similar heights reported by Satake et al. [67]. Furthermore, the material efficiency of the upper-bound design is safeguarded by

Table 2: Cross sections of the upper-bound WLSS design of the case-study building.

Floor number	Upper-bound optimal design $f_1 = 1.186$ Hz, self-weight = 992.2 Mg				
	Groups of beams (standard UB)		Groups of columns (welded SHS)		
	Inner	Edge	Central	Corner	Perimetric
1–3	UB1016 × 305 × 437	UB1016 × 305 × 272	w720 *t*32	w630 *t*32	w830 *t*40
4–6	UB1016 × 305 × 349	UB914 × 305 × 253	w610 *t*30	w520 *t*25	w640 *t*32
7–9	UB1016 × 305 × 349	UB914 × 305 × 224	w600 *t*30	w430 *t*22	w540 *t*28
10–12	UB914 × 305 × 289	UB914 × 305 × 201	w560 *t*28	w350 *t*18	w490 *t*25
13–15	UB610 × 305 × 238	UB686 × 254 × 125	w480 *t*25	w290 *t*15	w400 *t*20

the optimal sizing method used in the design. Importantly, the self-weight of the upper-bound design is $M(\mathbf{a}) = 992.2$ Mg, about 4.75 times heavier than the initial (lower-bound) design. In this respect, the herein adopted case-study building can serve as an interesting and realistic testbed of a code-compliant, material-efficient structure for demonstrating the practical merit and benefits of the proposed framework in Section 2 for reducing structural material use (and thus embodied carbon) in VS-sensitive ordinary high-rise buildings by employing DVAs to meet the crosswind serviceability criterion.

5.2. Adopted DVAs. The potential of two different types of DVAs is considered to reduce the structural material usage of the upper-bound WLSS design in Table 2. The first is a conventional passive linear top-floor TMD, graphically shown in Figure 4(a), which is, arguably, the most commonly considered DVA in practice for wind-borne motion control in tall buildings (e.g., [18, 21]). In this regard, it is of great practical interest to assess its potential for the task at hand, given the significant experience among design engineers and consultants of high-rise buildings with TMDs. The second is a passive linear ground-floor TID, graphically shown in Figure 4(b), whose potential for building motion control under lateral dynamic loads has been recently established in the scientific literature through numerical (e.g., [26, 68, 69]) and experimental (e.g., [55, 70, 71]) research work for seismic ground motions, but not for wind-excited structures. Notably, installing a TID on the ground floor offers additional advantages over the top-floor TMD placement, such as better accessibility for DVA installation, tuning/retuning, and maintenance, as well as the possibility for device upgrades (e.g., replacing with a larger inerter) to meet more stringent performance criteria (than those considered in the initial design) due to changes to the surrounding built environment, causing increased wind exposure (see, e.g., [22]).

The optimal tuning of both the adopted DVAs pertains to finding the optimal damping and stiffness coefficients of the linear dashpot and spring elements as shown in Figure 4. In terms of the inertia DVA property, m_{DVA}, it coincides to the secondary mass, m_{TMD}, for the TMD, while for the TID configuration of Figure 4(b), m_{DVA} coincides with the inertance property b. This is because the dynamic behaviour of the ideal grounded inerter element maps directly to a mass with inertia equal to the device inertance (see, e.g., [26, 29]).

5.3. Integrated Optimal Design of Case-Study TMD/TID-Equipped WLSS and Assessment. With upper and lower-bound WLSS designs specified, a series of minimum-weight designs are obtained using the sizing algorithm in Section 3 for 9 different target frequency values, equally spaced by approximately 0.10 Hz, within the frequency range [0.288 Hz, 1.186 Hz] (see Section 5.1). Figure 1(b) plots all the 10 minimum-weight WLSS designs plus the low-bound design from which only one (i.e., the upper-bound design with $f_1 = 1.186$ Hz) is code-compliant. Furthermore, Figure 1(c) plots the self-weight, $M(\mathbf{a})$, of these designs against f_1 and indicates that there is approximately a positive linear relationship between $M(\mathbf{a})$ and f_1, showing that the WLSS of the case-study building requires on average 84.1 additional Mg of steel to achieve lateral stiffening corresponding to a 0.1 Hz increase in the fundamental frequency.

The 10 code-deficient WLSS designs are equipped with either a top-floor TMD or a ground-floor TID which are optimally tuned for minimizing floor accelerations (see Section 4) under the design wind excitation in Figure 3(c). For each WLSS, TMDs and TIDs with 9 different inertial values equally spaced within a range of $[m_{\mathrm{DVA}}{}^{\min}, m_{\mathrm{DVA}}{}^{\max}]$ are considered. For both types of DVAs, the lower bound, $m_{\mathrm{DVA}}{}^{\min}$, of the inertia property range is notionally taken equal to zero to represent the uncontrolled WLSS. The upper bound, $m_{\mathrm{DVA}}{}^{\max}$, is defined separately for each DVA type as discussed in Section 2.3, that is, by setting it equal to the minimum required DVA inertia property to ensure that the lower-bound WLSS design in Table 1 satisfies the criterion in (17). This is herein accomplished by solving the optimal DVA design problem in (12) for several closely spaced values of m_{DVA} until the required m_{DVA} for which $\sigma_{\ddot{x}_{14}} = \exp(-3.65 - 0.41 \ln(0.288))$ holds is determined. It is found that $m_{\mathrm{DVA}}{}^{\max} = 2.83$ Mg for the TMD and $m_{\mathrm{DVA}}{}^{\max} = 596.1$ Mg for the TID. Notably, $m_{\mathrm{DVA}}{}^{\max}$ for the TMD is approximately 0.3% the self-weight of the "heavy" upper-bound uncontrolled WLSS in Table 2 and 1.5% the self-weight of the "light" lower-bound uncontrolled WLSS in Table 1. These TMD mass ratios span a reasonable range of real-life TMD implementation in existing buildings (e.g., [18, 19, 21, 48]). Accordingly, the $m_{\mathrm{DVA}}{}^{\max}$ value for the TID inertance is also reasonable (i.e., two orders of magnitude larger than the heavier considered TMD), since inertance of actual inerter devices scales up practically independently of the device physical mass based on different technologies/embodiments (e.g., [30]). Indeed, inerter prototypes for large scale (civil engineering) applications with inertance of up to 10,000 Mg have been reported in the literature (e.g., [55]).

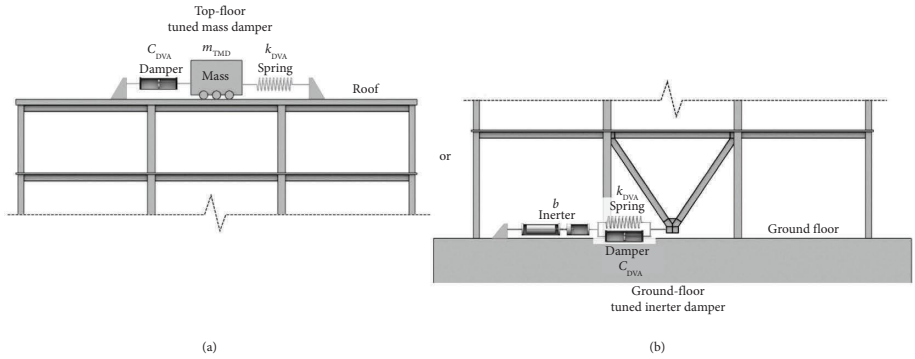

Figure 4: Schematic illustration of (a) top-floor tuned mass damper and (b) ground-floor tuned inerter damper.

Performance surfaces of the resulting $11 \times 9 = 99$ integrated optimally designed WLSS-plus-DVA systems are plotted in Figures 5(a) and 5(b) for TMD and TID absorbers, respectively, in terms of maximum RMS floor acceleration (always attained at the 14th floor of the case-study building) under the design wind excitation. These RMS values are computed using (14)–(16) as detailed in Section 4.2. It is found that RMS floor acceleration reduces monotonically with WLSS fundamental frequency and DVA inertia, but at reduced rates. These trends verify the opportunity of relaxing requirements for stiffening of WLSS by using a DVA with sufficient inertia to address human discomfort in the VS-sensitive case-study structure. To quantify this trade-off within a performance-targeted design context (i.e., aiming to achieve a preset performance level), the ISO6897 : 1984 wind comfort demand threshold in equation (17) is included in Figures 5(a) and 5(b) as a surface and its intersection with the performance surface is highlighted by a dotted curve. The latter curve delimits the acceptable (code-compliant) WLSS-plus-DVA designs located on the performance surface below the ISO6897 : 1984 demand surface from non-acceptable (code-deficient) designs located on the performance surface above the ISO6897 : 1984 demand surface. Clearly, the acceptable designs are conservative and can be further improved by reducing the stiffness of the WLSS and/or by reducing the inertia of the DVA. More importantly, Figures 5(a) and 5(b) show that code-compliant performance for wind habitability can be achieved using different sets of values for WLSS lateral stiffness (expressed through the natural frequency f_1) and DVA inertia. This consideration ultimately enables the self-weight reduction of the WLSS in VS-sensitive buildings.

To quantify the achieved steel tonnage reduction for the case-building, Figures 5(a) and 5(b) are projected onto the $M(\mathbf{a})$-m_{DVA} plane in Figures 5(c) and 5(d). On this plane, the intersection of the performance surface with the demand surface becomes a curve of non-dominated optimal design points for the bi-objective optimization problem in (2) for which no further self-weight reduction can be achieved without increasing the DVA inertia (either the secondary mass for the TMD or the inertance for the TID) and vice versa. Thus, the latter curve is a Pareto optimal front quantifying the optimal trade-off between the required WLSS material usage (steel tonnage) and the DVA inertia to achieve compliance to ISO6897 : 1984. While a design engineer can choose to implement any of the optimal designs lying on the two Pareto fronts, the extreme end of the Pareto fronts is herein highlighted corresponding to the most lightweight possible code-compliant WLSS design to Eurocode 3 [65] and ISO6897 : 1984 codes [6] (i.e., the lower-bound design in Table 1). The latter design achieves 68.4% self-weight reduction (i.e., 782.9 Mg savings in steel tonnage) compared to the upper-bound WLSS design for the case-study building. This remarkable reduction in material usage is achieved either by an optimally tuned TMD with 2.83 Mg additive secondary mass attached to the roof or by an optimally tuned ground-floor TID with inertance of 596.1 Mg, which are both practically reasonable and feasible DVAs based on the available technology as previously discussed. To this end, it is worth noting that no further WLSS self-weight reduction gains can be achieved beyond the lower end of the Pareto front by increasing further the DVA inertia properties within the proposed optimization-driven design framework, as lighter WLSS would not satisfy the ultimate limit state design requirements based on Eurocode 3 [65].

To gain an appreciation of the embodied carbon savings achieved by the WLSS-plus-DVA optimal design framework for the case-study building, a third axis normal to the $M(\mathbf{a})$-m_{DVA} plane is added to Figures 5(c) and 5(d) measuring embodied carbon CO_2 emissions, E_{CO2}, of the WLSS. The latter has been estimated using the expression

$$E_{\mathrm{CO}_2} = \left(1 + R_{\mathrm{wf}}\right)\left(M_{\mathrm{op}} \sum_{i=1}^{2} E_{\mathrm{op},i} + M_{\mathrm{cl}} \sum_{i=1}^{2} E_{\mathrm{cl},i}\right), \tag{18}$$

where M_{op} and M_{cl} represent the steel tonnage of beams (open UB sections) and columns (close SHS sections) used in the WLSS of the case-study building, respectively (Appendix B), and R_{wf} is the waste rate equal to 1% for steel frame structures according to Gibbons and Orr [72]. Furthermore, $E_{\mathrm{op},1}$ and $E_{\mathrm{op},2}$ are the embodied CO_2 emissions due to manufacturing (from cradle to gate) and transportation (from gate to site) for open steel sections, respectively, while $E_{\mathrm{cl},1}$ and $E_{\mathrm{cl},2}$ are the same for close steel sections, all taken from [72]. Note that in (18), the embodied CO_2 emissions due to construction and other site activities are neglected, as they only account for a small percentage of the total embodied carbon in typical building projects [72],

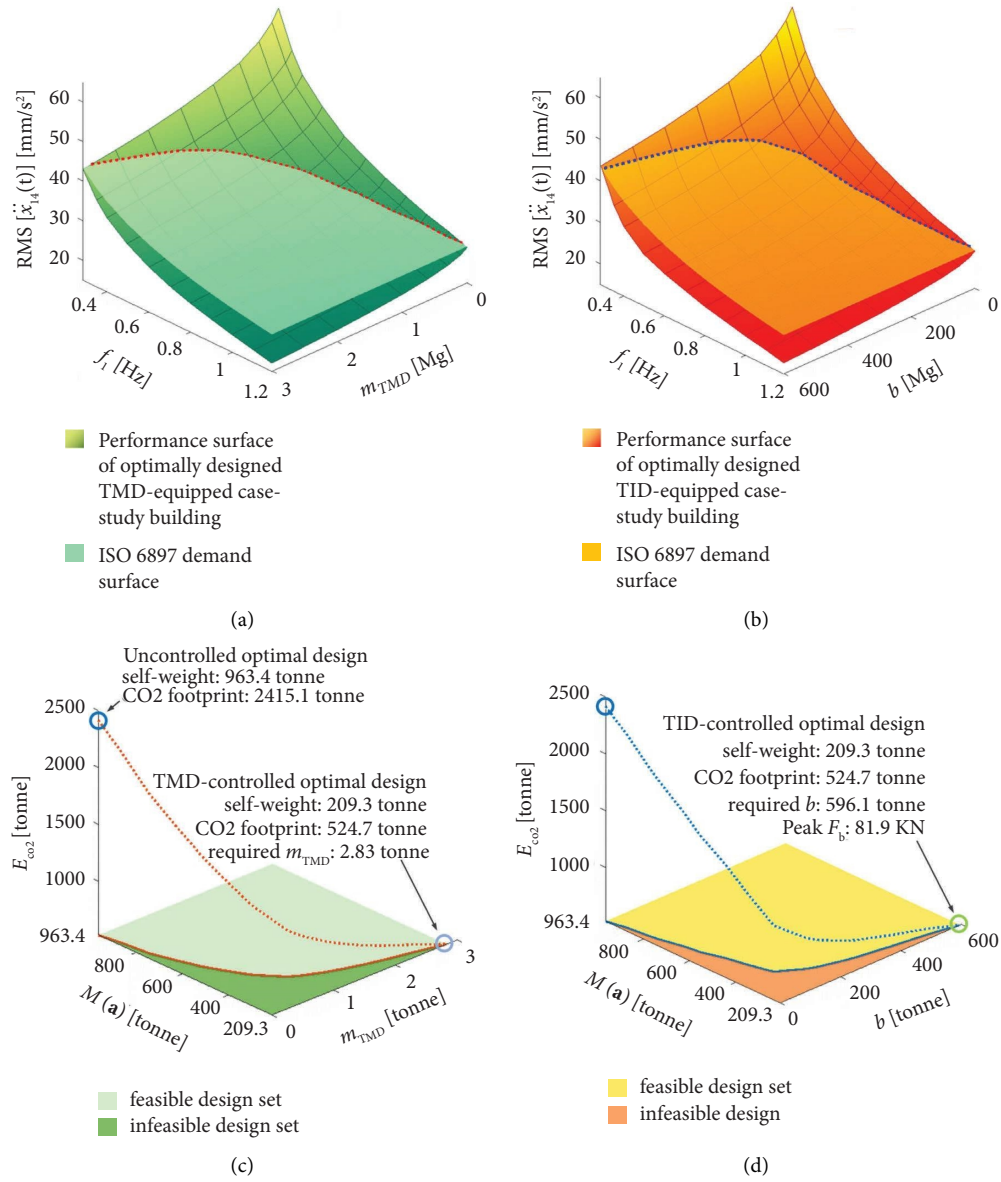

Figure 5: ISO6897 [6] occupant comfort threshold surface versus performance surfaces of optimally designed case-study building in Figure 2(a) equipped with an optimally tuned (a) top-floor TMD and (b) ground-floor TID. Embodied carbon emissions and trade-offs between structural self-weights and DVA inertial values of optimally designed case-study building equipped with an optimally tuned (c) top-floor TMD and (d) ground-floor TID.

and the same holds for the embodied CO_2 emissions of the DVAs. Under these assumptions, it is found that the previously discussed 782.9-tonne steel saving in the WLSS is equivalent to a 1989.0-tonne reduction in embodied CO_2 emissions, corresponding to the consumption of 855237.4 litres of 100% mineral petrol or 10.6 million km of medium car driving, based on published data in [73].

Finally, from the upfront monetary cost viewpoint, the WLSS-plus-DVA optimal design with a 2.83-tonne TMD is estimated to reduce the upfront monetary structural material cost by £1,558,102 or 68.2% compared to the upper-bound WLSS design (no DVA). This significant cost reduction has been estimated based on published data by Tse et al. [48] and by the Steel Construction Institute in UK [74], providing TMD cost per tonne of secondary mass and construction steel cost per tonne, respectively. For the case of the TID design with 596.1 t of inertance, cost reduction is expected to be even higher since the upfront cost of such an inerter device, though not yet commercially available, is expected to be similar to the cost of a standard viscous fluid damper device, since the peak inerter force developed is 81.9 kN, which can be readily transmitted to the building foundation without any special structural provisions. As a final remark, it is important to note that while DVAs with $m_{\mathrm{DVA}}{}^{\max}$ inertia are readily achievable for the herein considered case-study building and TMD/TID, this may not always be practically feasible for structures requiring excessively large $m_{\mathrm{DVA}}{}^{\max}$ inertia due to technological or

Table 3: Formulas relating different sectional properties to cross section areas for steel UB and SHS sections used in the WLSS of the case-study building in Figure 3(a).

	MRF beams (standard UB sections)	MRF columns (welded SHS sections)
Section illustration	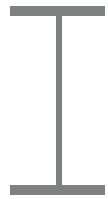	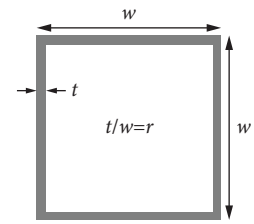
$A_{yy,n}$	$0.5542a_n + 78.1550$	$(2r/1-(1-2r)^2)a_n$
$A_{zz,n}$	$0.5132a_n + 295.1800$	
$I_{yy,n}$	$-5\times10^{-5}a_n^3 + 5.627a_n^2 - 15746a_n + 10^7$	$(1/12)\cdot(1+(1-2r)^2/1-(1-2r)^2)a_n^2$
$I_{zz,n}$	$-2\times10^{-6}a_n^3 + 0.1642a_n^2 + 911a_n - 6\times10^6$	
$J_{t,n}$	$2\times10^{-7}a_n^3 - 0.0027a_n^2 + 110.32a_n - 325619$	$(1/6)\cdot(1+(1-2r)^2/1-(1-2r)^2)a_n^2$

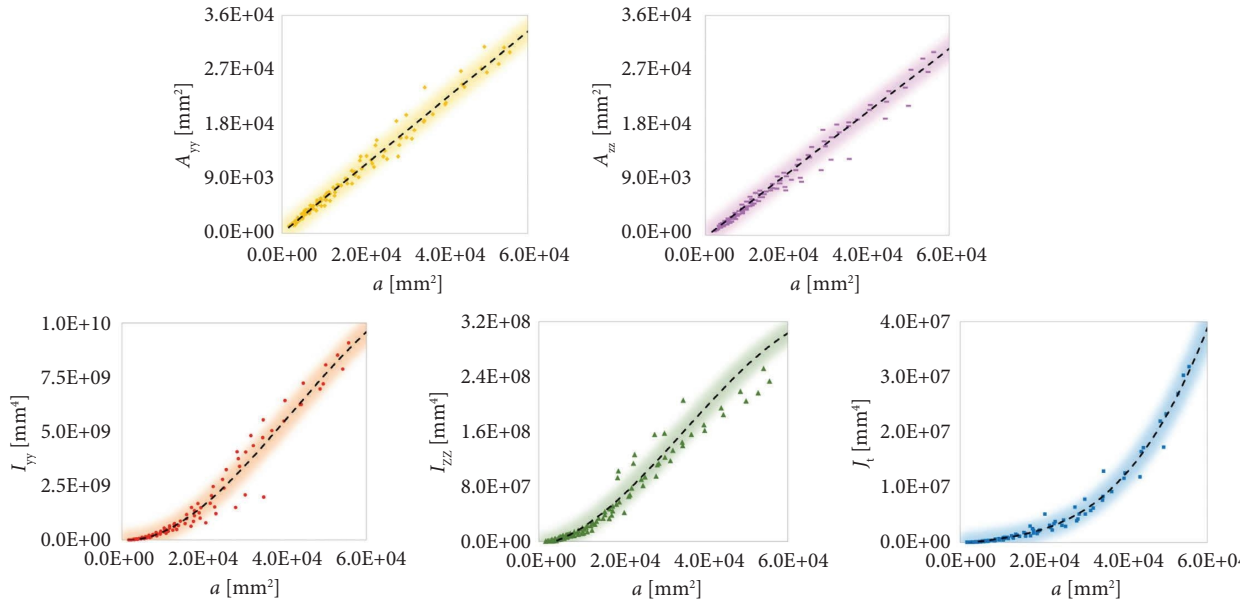

Figure 6: Statistical curve fitting of different sectional properties as polynomial functions of cross-sectional areas given in Table B1 based on data from standard UB sections [76].

monetary (upfront cost) limitations. For such structures, the design engineer may choose to consider an optimal design point on the Pareto front corresponding to a practically/economically feasible $m_{\mathrm{DVA}} < m_{\mathrm{DVA}}{}^{\max}$ value which would achieve lower self-weight gains from the one that would be achieved by a DVA with $m_{\mathrm{DVA}}{}^{\max}$ inertia property.

6. Concluding Remarks

The potential of using dynamic vibration absorbers (DVAs) for reducing the structural weight of wind load-resisting structural systems (WLSSs) and the associated embodied carbon footprint in routine vortex shedding (VS)-sensitive high-rise buildings has been numerically established. This was achieved by formulating a novel bi-objective constrained optimization design framework for the integrated WLSS-plus-DVA minimum-weight design to meet crosswind occupant comfort serviceability criteria which govern the global structural design. Furthermore, a versatile numerical strategy has been proposed for the solution of the optimization-driven design framework by application of standard structural sizing optimization and optimal DVA tuning approaches in a non-iterative and parallelizable fashion. Thus, the proposed solution strategy allows for a computationally efficient and readily implementable application of the integrated design framework by leaving significant leeway to structural designers to choose structural sizing and DVA tuning algorithms, separately, from those available in commercial and/or research software. In the paper, a computationally efficient optimality-criteria (OC)-based approach was used for minimal WLSS sizing with a frequency constraint, and a non-gradient-based pattern search algorithm was used for optimal DVA

design to minimize building floor accelerations to design crosswind forces accounting for VS effects.

The applicability of the proposed integrated design framework and numerical solution strategy were exemplified using a 15-storey steel moment-resisting frame building designed for structural serviceability and safety as per Eurocode 3 [65] and equipped with two different DVAs: a conventional top-floor tuned mass damper (TMD) or a ground-floor tuned inerter damper (TID). For each type of DVAs, Pareto optimal integrated WLSS-plus-DVA designs were obtained to demonstrate a remarkably positive trade-off between the steel WLSS self-weight and DVA inertia property in meeting the serviceability occupant wind comfort criterion of the ISO6897 building standard [6]. It was shown that several hundred tonnes of structural steel can be saved from the WLSS of the case-study building in meeting occupant wind comfort requirements by using either a standard linear passive top-floor TMD (with less than 3 tonne of mass) or a ground-floor TID with inertance of a few hundreds of tonnes. The latter consideration suggests that inerter-based DVAs used in conjunction with the herein proposed framework may be a quite promising new technology for reducing structural material usage and embodied carbon in wind-sensitive slender high-rise buildings.

Nevertheless, it is recognized that the reported numerical results pertain to a single benchmark structure. Although this structure is representative of modern steel high-rise buildings, further research work is warranted to quantify the gains of using different types of DVAs in terms of structural material usage, construction cost, and embodied carbon to different types of WLSSs in high-rise buildings including reinforced concrete, braced steel, concrete-steel composite, and mass timber structures. In this respect, the proposed framework may be further tailored and extended to directly minimize the environmental impact (embodied carbon) and/or the construction cost of buildings depending on the construction material and DVA type. Furthermore, the possibility of extending the framework and solution strategy to encompass topology optimization aspects as well as a wider range of energy dissipation devices for building lateral motion control is also a promising direction for future rewarding research. In this regard, it is envisioned that the herein introduced integrated WLSS-DVA design framework is agenda-setting, serving as a steppingstone towards reconciling vibration control with structural optimization to achieve ever more resilient (to critical wind loads) and material-efficient building structures.

Appendix

A. Crosswind Excitation Model Accounting for VS Effects

The crosswind forces exerted on buildings are commonly modelled as a zero-mean Gaussian ergodic spatially correlated random field expressed in frequency domain through a power spectral density matrix (PSDM), $\mathbf{S_{FF}}$. In the illustrative example (Section 5), the analytical PSDM model of Liang et al. [3] for tall buildings with rectangular footprint is adopted. For the case-study building with a total height of 49.8 m and a square footprint, the diagonal elements of the PSDM are given as

$$\mathbf{S_{FF}}(\omega)[q,q] = \frac{\sigma_q^2}{\omega}\left[\frac{0.1357\left(\omega/\omega_q\right)^2}{\left(1-\left(\omega/\omega_q\right)^2\right)^2 + 0.0630\left(\omega/\omega_q\right)^2} + \frac{0.2008\left(\omega/\omega_q\right)^3}{\left(1-\left(\omega/\omega_q\right)^2\right)^2 + 2\left(\omega/\omega_q\right)^2}\right], q = 1, 2, 15, \tag{A.1}$$

which specify the PSD function of the wind force acting at the q-th floor slab located at height z_q from the ground. In the previous expression, ω_q is the VS frequency at z_q height and σ_q is the RMS of the crosswind force at the q-th floor slab given as

$$\sigma_q = \frac{1}{2}\rho v_{\mathrm{m}}^2\left(z_q\right)\overline{C}_{\mathrm{L}} B \Delta z_q, \tag{A.2}$$

where ρ is the air density taken equal to 1.25 kg/m^3, $\overline{C}_{\mathrm{L}}$ is the mean RMS lift coefficient equal to 0.404 for square footprint buildings, B is the building width in the across-wind direction, Δz_q is the tributary height of the q-th floor taken as half the storey height above floor q plus half the storey height below floor Q, and $\mathrm{v_m}(z_q)$ is the mean wind velocity at z_q height. The latter is determined by [66]

$$v_{\mathrm{m}}(z) = c_{\mathrm{r}}(z) c_{\mathrm{o}}(z) v_{\mathrm{b}}, \tag{A.3}$$

where V_b is the basic wind velocity (i.e., the 10 min mean wind velocity at 10m above open flat country terrain) taken equal to 20 m/s, $c_{\mathrm{o}}(z)$ is the orography factor assumed equal to 1.0, and $c_{\mathrm{r}}(z)$ is the roughness factor based on the Eurocode 1-compliant logarithmic law and terrain category IV (i.e., urban area in which at least 15% of the surface is covered with buildings and their average height exceeds 15 m). Furthermore, the VS frequency is determined by

$$\omega_q = \frac{2\pi S_{\mathrm{t}} v_{\mathrm{m}}\left(z_q\right)}{B}, \tag{A.4}$$

in which S_{t} is the Strouhal number taken equal to 0.084 as experimentally determined by Liang et al. [3] for square footprint tall buildings. The off-diagonal terms of the PSDM modelling the spatial correlation of wind forces acting at floor slabs k and l are given as [3]

$$S_{FF}[k,l] = \exp\left[-\left(\frac{z_k - z_l}{91.74}\right)^2\right]\sqrt{S_k(\omega) S_l(\omega)}. \tag{A.5}$$

B. Expressing Sectional Properties in terms of Cross-Sectional Area

To use the iterative sizing algorithm in Section 3.2 for minimum-weight design of the case-study building's WLSS, it is necessary to express all the remaining sectional properties of each group of structural members as functions of the cross-sectional areas, a_n ($n = 1, \ldots, 25$), taken as structural DVs (e.g. [75]). There are 5 such sectional properties per member group: shear areas $A_{yy,n}$ and $A_{zz,n}$ along the cross section's local y-y and z-z axes, respectively, second moments of inertia $I_{yy,n}$ and $I_{zz,n}$ about the major/y-y and minor/z-z bending axes, respectively, and polar moment of inertia $J_{t,n}$.

For standard commercial UB steel sections used in the beam members of the case-study building, different polynomial expressions, reported in Table 3, are derived to relate each of the 5 previous sectional properties to a_n by least-squares fitting to sectional data [76], as shown in Figure 6. Columns of the case study are made of welded SHS sections with fixed ratio of plate thickness, t, over outer dimension, w, for which exact analytical expressions, reported in Table 3, are derived to relate the 5 sectional properties to the corresponding cross-sectional areas.

C. Low-Order Representation of DVA-Equipped Case-Study Building

To facilitate random vibration analysis of the case-study building in Figure 3(a) for crosswind excitation, planar low-order dynamic models are derived from the detailed finite element models of the WLSS designs, with 15 translational DOFs (one per floor) along a principal building axis. The low-order models are defined in terms of lumped/diagonal mass, $\mathbf{M}_s^{15} \in \mathbb{R}^{15\times15}$, damping $\mathbf{C}_s^{15} \in \mathbb{R}^{15\times15}$, and stiffness $\mathbf{K}_s^{15} \in \mathbb{R}^{15\times15}$ matrices which can be used in conjunction with (14)–(16) to find RMS floor acceleration to crosswind forces defined by means of the $\mathbf{S_{FF}}$ PSDM defined in Appendix A. The mass matrix, $\mathbf{M}_s^{15}$, collects the floor masses for the nominal gravitational load combination per Eurocode 1 [66] (permanent plus 30% variable actions). Then, the full stiffness matrix, $\mathbf{K}_s^{15}$, is derived such that the natural frequencies and undamped mode shapes of the low-order model match exactly those of the first 15 global lateral/translational vibration modes of the detailed FEM. This is achieved by solving the following system of eigenvalue equations:

$$\left(\mathbf{K}_s^{15} - \omega_{\mathrm{FEM},l}^2 \mathbf{M}_s^{15}\right)\boldsymbol{\varphi}_{\mathrm{FEM},l} = 0\,(l = 1, 15), \tag{C.1}$$

for $\mathbf{K}_s^{15}$, in which the vector $\boldsymbol{\varphi}_{\mathrm{FEM},l} \in \mathbb{R}^{15\times1}$ collects the l-th translational mode shape (at the centre of each floor slab) of the detailed FEM along a building principal axis and $\omega_{\mathrm{FEM},l}$ is the corresponding circular natural frequency (see also [22]). Lastly, the damping matrix, $\mathbf{C}_s^{15}$, is defined as (e.g., [77])

$$\mathbf{C}_s^{15} = \left(\boldsymbol{\Phi}^T\right)^{-1} \mathbf{C}_{\mathrm{mod}} \left(\boldsymbol{\Phi}\right)^{-1}, \tag{C.2}$$

where $\Phi \in \mathbb{R}^{15\times15}$ is the modal shape matrix collecting all 15 mode shapes of the low-order model and $\mathbf{C}_{\mathrm{mod}} \in \mathbb{R}^{15\times15}$ is a diagonal matrix with main diagonal elements

$$\mathbf{C}_{\mathrm{mod}}[l,l] = 2\omega_l \xi_l \left(\boldsymbol{\varphi}_l^T \mathbf{M}_s^{15} \boldsymbol{\varphi}_l\right)(l = 1, 15), \tag{C.3}$$

in which ω_l is the l-th circular natural frequency of the low-order model and ξ_l is the corresponding modal damping ratio. The latter is taken equal to 1% for the first mode shape in line with ISO 4354 : 2009 guidelines for steel buildings. Increasing modal damping ratios for higher modes are assumed, equal to 2% for $l = 2,3$; 4% for $l = 4,5,6$; 8% for $l = 7,8,9$; 16% for $l = 10,11,12$; and 32% for $l = 13,14,15$, to account for the anticipated greater participation of non-structural components in the inherent structural damping higher mode oscillations (see [78] and reference therein).

The mass, damping, and stiffness matrices of the low-order WLSS model equipped with either a top-floor TMD or a ground-floor TID used in the illustrative example (Section 5.3) can be written as

$$\begin{aligned}
\mathbf{M}_{\mathrm{low}} &= \mathbf{M}_s^{16} + m_{\mathrm{DVA}} \mathbf{I}_{16} \mathbf{I}_{16}^T, \\
\mathbf{C}_{\mathrm{low}} &= \mathbf{C}_s^{16} + c_{\mathrm{DVA}} \left(\mathbf{I}_{16} \mathbf{I}_{16}^T + \mathbf{I}_d \mathbf{I}_d^T - \mathbf{I}_d \mathbf{I}_{16}^T - \mathbf{I}_{16} \mathbf{I}_d^T\right), \\
\mathbf{K}_{\mathrm{low}} &= \mathbf{K}_s^{16} + k_{\mathrm{DVA}} \left(\mathbf{I}_{16} \mathbf{I}_{16}^T + \mathbf{I}_d \mathbf{I}_d^T - \mathbf{I}_d \mathbf{I}_{16}^T - \mathbf{I}_{16} \mathbf{I}_d^T\right),
\end{aligned} \tag{C.4}$$

where the subscript "d" denotes the number of the floor on which the DVA is installed. For top-floor TMD, $d = 15$, while for ground-floor TID, $d = 1$. In (C.4), the column vectors $\mathbf{I}_d \in \mathbb{R}^{16\times1}$ and $\mathbf{I}_{16} \in \mathbb{R}^{16\times1}$ have zero entries except for the d-th and last entries, respectively, which are equal to one. Furthermore, $\mathbf{M}_s^{16} \in \mathbb{R}^{16\times16}$, $\mathbf{C}_s^{16} \in \mathbb{R}^{16\times16}$, and $\mathbf{K}_s^{16} \in \mathbb{R}^{16\times16}$ are $\mathbf{M}_s^{15}$, $\mathbf{C}_s^{15}$, and $\mathbf{K}_s^{15}$ matrices, respectively, augmented by an additional (bottom) row and (rightmost) column with zero entries. In this setting, the 16$^{\mathrm{th}}$ DOF of the low-order model of DVA-equipped WLSSs corresponds to the DVA. The latter is not subjected to an external wind load as the device is internally housed. Therefore, in using the matrices in (C.4) together with (16) to find RMS floor acceleration to crosswind forces, the excitation $\mathbf{S_{FF}}$ PSDM in (14) is augmented by an additional bottom row and a rightmost column with zero entries.

Data Availability

Numerical models of this research are available from the corresponding author upon request. All numerical data of this research are provided in the paper.

Conflicts of Interest

The authors declare that they have no conflicts of interest.

Acknowledgments

The second author gratefully acknowledges the support of the Engineering and Physical Sciences Research Council (EPSRC), U.K., under grant no. EP/M017621/1.

References

[1] S. Frolking, T. Milliman, K. C. Seto, and M. A. Friedl, "A global fingerprint of macro-scale changes in urban structure from 1999 to 2009," *Environmental Research Letters*, vol. 8, no. 2, Article ID 024004, 2013.

[2] R. Mahtta, A. Mahendra, and K. C. Seto, "Building up or spreading out? Typologies of urban growth across 478 cities of 1 million+," *Environmental Research Letters*, vol. 14, no. 12, Article ID 124077, 2019.

[3] S. G. Liang, S. C. Liu, Q. S. Li, L. L. Zhang, and M. Gu, "Mathematical model of acrosswind dynamic loads on rectangular tall buildings," *Journal of Wind Engineering and Industrial Aerodynamics*, vol. 90, no. 12-15, pp. 1757–1770, 2002.

[4] E. Simiu and R. H. Scanlan, *Wind Effects on Structures: Fundamentals and Applications to Design*, John Wiley & Sons, Hoboken, NJ, USA, 1996.

[5] K. C. S. Kwok, P. A. Hitchcock, and M. D. Burton, "Perception of vibration and occupant comfort in wind-excited tall buildings," *Journal of Wind Engineering and Industrial Aerodynamics*, vol. 97, no. 7-8, pp. 368–380, 2009.

[6] International Organization of Standardization, "Guidelines for the evaluation of the response of occupants of fixed structures, especially buildings and off-shore structures, to low frequency horizontal motion (0.063 to 1 Hz)," 1984, https://www.iso.org/standard/13419.html.

[7] Architectural Institute of Japan Recommendations, *Guidelines for the Evaluation of Habitability to Building Vibration*, Architectural Institute of Japan Recommendations, Tokyo, 2004.

[8] F. Petrini and M. Ciampoli, "Performance-based wind design of tall buildings," *Struct. Infrastruct. Eng.*vol. 8, no. 10, pp. 954–966, 2012.

[9] E. Bernardini, S. M. J. Spence, D. K. Kwon, and A. Kareem, "Performance-based design of high-rise buildings for occupant comfort," *Journal of Structural Engineering*, vol. 141, no. 10, 2015.

[10] B. S. Taranath, *Tall Building Design, Steel, concrete, and Composite Systems*, CRC Press, Boca Raton, FL, 2017.

[11] P. Chastas, T. Theodosiou, and D. Bikas, "Embodied energy in residential buildings towards the nearly zero energy building: a literature review," *Building and Environment*, vol. 105, pp. 267–282, 2016.

[12] M. Robati, P. Oldfield, A. A. Nezhad, D. G. Carmichael, and A. Kuru, "Carbon value engineering: a framework for integrating embodied carbon and cost reduction strategies in building design," *Building and Environment*, vol. 192, Article ID 107620, 107620 pages, 2021.

[13] P. Foraboschi, M. Mercanzin, and D. Trabucco, "Sustainable structural design of tall buildings based on embodied energy," *Energy and Buildings*, vol. 68, pp. 254–269, 2014.

[14] V. J. L. Gan, C. M. Chan, K. T. Tse, I. M. C. Lo, and J. C. P. Cheng, "A comparative analysis of embodied carbon in high-rise buildings regarding different design parameters," *Journal of Cleaner Production*, vol. 161, pp. 663–675, 2017.

[15] Z. S. Moussavi Nadoushani and A. Akbarnezhad, "Effects of structural system on the life cycle carbon footprint of buildings," *Energy and Buildings*, vol. 102, pp. 337–346, 2015.

[16] International Energy Agency (Iea), "Global Status Report 2019 for Buildings and Construction - towards a Zero Emission, Efficient, and Resilient Buildings and Construction Sector, UN Environment Programme," 2019, https://www.worldgbc.org/news-media/2019-global-status-report-buildings-and-construction.

[17] United Nations Department of Economic and Social Affairs (Un Desa), *World urbanization prospects: the 2018 revision*, United Nations Department of Economic and Social Affairs (Un Desa), New York, NY, USA, 2018.

[18] A. Kareem, T. Kijewski, and Y. Tamura, "Mitigation of motions of tall buildings with specific examples of recent applications," *Wind and Structures*, vol. 2, no. 3, pp. 201–251, 1999.

[19] Q. S. Li, L.-H. Zhi, A. Y. Tuan, C.-S. Kao, S.-C. Su, and C.-F. Wu, "Dynamic behavior of taipei 101 tower: field measurement and numerical analysis," *Journal of Structural Engineering*, vol. 137, no. 1, pp. 143–155, 2011.

[20] Q. Zhang, X. Luo, J. Ding, B. Xie, and X. Gao, "Dynamic response evaluation on TMD and main tower of Shanghai Tower subjected to Typhoon In-Fa," *The Structural Design of Tall and Special Buildings*, vol. 31, no. 9, 2022.

[21] S. Elias and V. Matsagar, "Research developments in vibration control of structures using passive tuned mass dampers," *Annual Reviews in Control*, vol. 44, pp. 129–156, 2017.

[22] A. Giaralis and F. Petrini, "Wind-induced vibration mitigation in tall buildings using the tuned mass-damper-inerter," *Journal of Structural Engineering*, vol. 143, no. 9, 2017.

[23] Q. Wang, H. Qiao, D. De Domenico, Z. Zhu, and Z. Xie, "Wind-induced response control of high-rise buildings using inerter-based vibration absorbers," *Applied Sciences*, vol. 9, no. 23, p. 5045, 2019.

[24] F. Petrini, A. Giaralis, and Z. Wang, "Optimal tuned mass-damper-inerter (TMDI) design in wind-excited tall buildings for occupants' comfort serviceability performance and energy harvesting," *Engineering Structures*, vol. 204, Article ID 109904, 109904 pages, 2020.

[25] Z. Wang and A. Giaralis, "Top-story softening for enhanced mitigation of vortex shedding-induced vibrations in wind-excited tuned mass damper inerter-equipped tall buildings," *Journal of Structural Engineering*, vol. 147, no. 1, 2021.

[26] I. F. Lazar, S. A. Neild, and D. J. Wagg, "Using an inerter-based device for structural vibration suppression," *Earthquake Engineering & Structural Dynamics*, vol. 43, no. 8, pp. 1129–1147, 2014.

[27] L. Marian and A. Giaralis, "Optimal design of a novel tuned mass-damper–inerter (TMDI) passive vibration control configuration for stochastically support-excited structural systems," *Probabilistic Engineering Mechanics*, vol. 38, pp. 156–164, 2014.

[28] S. Y. Zhang, J. Z. Jiang, and S. Neild, "Optimal configurations for a linear vibration suppression device in a multi-storey building," *Structural Control and Health Monitoring*, vol. 24, no. 3, p. e1887, Article ID e1887, 2017.

[29] M. C. Smith, "Synthesis of mechanical networks: the Inerter," *IEEE Transactions on Automatic Control*, vol. 47, no. 10, pp. 1648–1662, 2002.

[30] M. C. Smith, "The inerter: a retrospective," *Annual Review of Control, Robotics, and Autonomous Systems*, vol. 3, no. 1, pp. 361–391, 2020.

[31] D. J. Wagg, "A review of the mechanical inerter: historical context, physical realisations and nonlinear applications," *Nonlinear Dynamics*, vol. 104, no. 1, pp. 13–34, 2021.

[32] C. M. Chan and J. K. L. Chui, "Wind-induced response and serviceability design optimization of tall steel buildings," *Engineering Structures*, vol. 28, no. 4, pp. 503–513, 2006.

[33] C. M. Chan, M. F. Huang, and K. C. S. Kwok, "Stiffness optimization for wind-induced dynamic serviceability design

of tall buildings," *Journal of Structural Engineering*, vol. 135, no. 8, pp. 985–997, 2009.

[34] J. Y. Fu, Q. Zheng, Y. Q. Huang, J. R. Wu, Y. L. Pi, and Q. X. Liu, "Design optimization on high-rise buildings considering occupant comfort reliability and joint distribution of wind speed and direction," *Engineering Structures*, vol. 156, pp. 460–471, 2018.

[35] S. M. J. Spence, "Optimization of uncertain and dynamic high-rise structures for occupant comfort: an adaptive kriging approach," *Structural Safety*, vol. 75, pp. 57–66, 2018.

[36] M. C. Moynihan and J. M. Allwood, "Utilization of structural steel in buildings," *Proceedings of the Royal Society A: Mathematical, Physical & Engineering Sciences*, vol. 470, no. 2168, Article ID 20140170, 2014.

[37] F. Pomponi and A. Moncaster, "Embodied carbon mitigation and reduction in the built environment - what does the evidence say?" *Journal of Environmental Management*, vol. 181, pp. 687–700, 2016.

[38] J. Orr, M. P. Drewniok, I. Walker, T. Ibell, A. Copping, and S. Emmitt, "Minimising energy in construction: practitioners' views on material efficiency," *Resources, Conservation and Recycling*, vol. 140, pp. 125–136, 2019.

[39] J. M. Allwood, M. F. Ashby, T. G. Gutowski, and E. Worrell, "Material efficiency: a white paper," *Resources, Conservation and Recycling*, vol. 55, no. 3, pp. 362–381, 2011.

[40] J. Grinham, H. Fjeldheim, B. Yan et al., "Zero-carbon balance: the case of house zero," *Building and Environment*, vol. 207, no. 6, Article ID 108511, 2022.

[41] M. Garcia-Sanz, "Control Co-Design: an engineering game changer," *Adv Control Appl*, vol. 1, p. e18, 2019.

[42] D. De Domenico, G. Ricciardi, and I. Takewaki, "Design strategies of viscous dampers for seismic protection of building structures: a review," *Soil Dynamics and Earthquake Engineering*, vol. 118, pp. 144–165, 2019.

[43] H. Akehashi and I. Takewaki, "Simultaneous optimization of elastic-plastic building structures and viscous dampers under critical double impulse," *Front. Built Environ*, vol. 6, Article ID 623832, 2020.

[44] S. Javadinasab Hormozabad and M. Gutierrez Soto, "Performance-based control co-design of building structures with controlled rocking steel braced frames via neural dynamic model," *Structural and Multidisciplinary Optimization*, vol. 64, no. 3, pp. 1111–1125, 2021.

[45] I. Takewaki and H. Akehashi, "Comprehensive review of optimal and smart design of nonlinear building structures with and without passive dampers subjected to earthquake loading," *Frontiers in Built Environment*, vol. 7, Article ID 631114, 2021.

[46] American Society of Civil Engineer, *Standard on Minimum Loads for the Design of Buildings and Other Structures*, Ascelibrary, Reston, VA, USA, 1995.

[47] L. G. Griffis, "Serviceability limit states under wind load," *Engineering Journal of American Institute of Steel Construction*, vol. 30, pp. 23–28, 1993.

[48] K. T. Tse, K. C. S. Kwok, and Y. Tamura, "Performance and cost evaluation of a smart tuned mass damper for suppressing wind-induced lateral-torsional motion of tall structures," *Journal of Structural Engineering*, vol. 138, no. 4, pp. 514–525, 2012.

[49] D. Mavrokapnidis, C. C. Mitropoulou, and N. D. Lagaros, "Environmental assessment of cost optimized structural systems in tall buildings," *Journal of Building Engineering*, vol. 24, Article ID 100730, 100730 pages, 2019.

[50] C. M. Chan, "Optimal lateral stiffness design of tall buildings of mixed steel and concrete construction," *The Structural Design of Tall Buildings*, vol. 10, no. 3, pp. 155–177, 2001.

[51] P. E. Mergos, "Seismic design of reinforced concrete frames for minimum embodied CO2 emissions," *Energy and Buildings*, vol. 162, pp. 177–186, 2018.

[52] V. J. L. Gan, C. L. Wong, K. T. Tse, J. C. P. Cheng, I. M. C. Lo, and C. M. Chan, "Parametric modelling and evolutionary optimization for cost-optimal and low-carbon design of high-rise reinforced concrete buildings," *Advanced Engineering Informatics*, vol. 42, Article ID 100962, 2019.

[53] H. L. Gauch, W. Hawkins, T. Ibell, J. M. Allwood, and C. F. Dunant, "Carbon vs. cost option mapping: a tool for improving early-stage design decisions," *Automation in Construction*, vol. 136, Article ID 104178, 2022.

[54] R. Ruiz, A. A. Taflanidis, A. Giaralis, and D. Lopez-Garcia, "Risk-informed optimization of the tuned mass-damper-inerter (TMDI) for the seismic protection of multi-storey building structures," *Engineering Structures*, vol. 177, pp. 836–850, 2018.

[55] S. Nakaminami, H. Kida, K. Ikago, and N. Inoue, "Dynamic testing of a full-scale hydraulic inerter-damper for the seismic protection of civil structures," in *Proceedings of the 7th International Conference on Advances in Experimental Structural Engineering*, M. Furinghetti, D. Bolognini, and A. Pavese, Eds., Eucentre foundation, Pavia, Italy, pp. 41–54, September 2107.

[56] D. Pietrosanti, M. De Angelis, and A. Giaralis, "Experimental seismic performance assessment and numerical modelling of nonlinear inerter vibration absorber (IVA)-equipped base isolated structures tested on shaking table," *Earthquake Engineering & Structural Dynamics*, vol. 50, no. 10, pp. 2732–2753, 2021.

[57] Z. Wang and K. D. Tsavdaridis, "Optimality criteria-based minimum-weight design method for modular building systems subjected to generalised stiffness constraints: a comparative study," *Engineering Structures*, vol. 251, Article ID 113472, 113472 pages, 2022.

[58] V. B. Venkayya, "Design of optimum structures," *Computers & Structures*, vol. 1, no. 1-2, pp. 265–309, 1971.

[59] V. B. Venkayya, "Optimality criteria: a basis for multidisciplinary design optimization," *Computational Mechanics*, vol. 5, no. 1, pp. 1–21, 1989.

[60] K. Svanberg, "On local and global minima in structural optimisation," in *New Directions in Optimum Structural Design*, E. Atrek, R. H. Gallagher, K. M. Ragsdell, and O. C. Zienkiewicz, Eds., Wiley–Blackwell, Hoboken, NJ, USA, 1984.

[61] P. Christensen and A. Klarbring, *An Introduction to Structural Optimisation*, Springer Dordrecht, Berlin/Heidelberg, Germany, 2009.

[62] W. H. Wittrick, "Rates of change of eigenvalues, with Reference to buckling and vibration problems," *The Journal of the Royal Aeronautical Society*, vol. 66, no. 621, pp. 590-591, 1962.

[63] C. Audet and J. E. Dennis, "Analysis of generalized pattern searches," *SIAM Journal on Optimization*, vol. 13, no. 3, pp. 889–903, 2002.

[64] M. Azizi, S. Talatahari, and A. Giaralis, "Optimization of engineering design problems using atomic orbital search algorithm," *IEEE Access*, vol. 9, pp. 102497–102519, 2021.

[65] Breeding Science, *British Standard Institution, Eurocode 3: Design of Steel Structures – Part 1-1: General Rules and Rules for Buildings*, Breeding Science, Kyoto, Japan, 1993.

[66] Breeding Science, *British Standard Institution, Eurocode 1: Actions on Structures – Part 1 – 4: General actions - Wind Actions*, Breeding Science, Kyoto, Japan, 1991.

[67] N. Satake, K. i. Suda, T. Arakawa, A. Sasaki, and Y. Tamura, "Damping evaluation using full-scale data of buildings in Japan," *Journal of Structural Engineering*, vol. 129, no. 4, pp. 470–477, 2003.

[68] A. Giaralis and A. Taflanidis, "Optimal tuned mass-damper-inerter (TMDI) design for seismically excited MDOF structures with model uncertainties based on reliability criteria," *Structural Control and Health Monitoring*, vol. 25, no. 2, Article ID e2082, e2082 pages, 2018.

[69] D. De Domenico and G. Ricciardi, "An enhanced base isolation system equipped with optimal tuned mass damper inerter (TMDI)," *Earthquake Engineering & Structural Dynamics*, vol. 47, no. 5, pp. 1169–1192, 2018.

[70] A. Gonzalez-Buelga, I. F. Lazar, J. Z. Jiang, S. A. Neild, and D. J. Inman, "Assessing the effect of nonlinearities on the performance of a tuned inerter damper," *Structural Control and Health Monitoring*, vol. 24, no. 3, p. e1879, Article ID e1879, 2017.

[71] D. De Domenico, P. Deastra, G. Ricciardi, N. D. Sims, and D. J. Wagg, "Novel fluid inerter based tuned mass dampers for optimised structural control of base-isolated buildings," *Journal of the Franklin Institute*, vol. 356, no. 14, pp. 7626–7649, 2019.

[72] O. P. Gibbons and J. J. Orr, "How to calculate embodied carbon, the institution of structural engineers," 2020, https://www.istructe.org/IStructE/media/Public/Resources/istructe-how-to-calculate-embodied-carbon.pdf.

[73] Department for Business, "Energy & industrial strategy (beis), greenhouse gas reporting: conversion 992 factors," 2021, https://www.gov.uk/government/publications/greenhouse-gas-reporting-conversion993factors-2021.

[74] S.C.. info, "Cost of structural steelwork," 2022, https://www.steelconstruction.info/Cost_of_structural_steelwork#Low_rise_and_short_span_buildings.

[75] C. M. Chan, D. E. Grierson, and A. N. Sherbourne, "Automatic optimal design of tall steel building frameworks," *Journal of Structural Engineering*, vol. 121, no. 5, pp. 838–847, 1995.

[76] EurocodeApplied, "Table of design properties for flanged steel profiles (IPE, HEA, HEB, HEM, UB, UC, UBP)," 2022, https://eurocodeapplied.com/design/en1993/ipe-hea-heb-hem-design-properties.

[77] A. K. Chopra, *Dynamics of Structures: Theory and Applications to Earthquake Engineering*, Prentice-Hall, U.S, Hoboken, NJ, USA, 2001.

[78] S. M. J. Spence and A. Kareem, "Tall buildings and damping: a concept-based data driven model," *Journal of Structural Engineering*, vol. 140, no. 5, 2014.